



Research Article

Computational molecular docking and simulation-based prediction of natural compounds from *Nyctanthes arbor-tristis* as potential antifungal agents

Sohail Akhtar^a, Varish Ahmad^b, Mohammad Aatif^c, Qazi Mohammad Sajid Jamal^{d,*}

^aHealth Information Management and Technology Department, College of Applied Medical Sciences, King Faisal University, Al-Ahsa 31982, Saudi Arabia

^bHealth Information Technology Department, The Applied College, King Abdulaziz University, Jeddah 21589, Saudi Arabia

^cDepartment of Public Health, King Faisal University, College of Applied Medical Sciences, Al Ahsa, 31982, Saudi Arabia

^dDepartment of Health Informatics, College of Applied Medical Sciences, Qassim University, Buraydah, 51452, Saudi Arabia

ARTICLE INFO

Keywords:

Drug discovery
Food and agriculture
Fungal inhibition
Molecular docking simulation
Nyctanthes arbor-tristis

ABSTRACT

Mycoses, or fungal illnesses, are common health problems that frequently impact crops, animals, and food. Molecular docking and dynamics simulation techniques were used to predict the multitargeted antifungal potential of phytochemicals from *Nyctanthes arbor-tristis* against multiple drug targets of fungi.

We analyzed the binding interaction and dynamics of phytochemicals of the *Nyctanthes arbor-tristis* plant with multiple drug targets of fungi through a computational study.

The strong binding affinities with the targets studied of fungi were found to be more significant compared to the reference drug (lupeol -11.5 kcal/mol; DB01263, a synthetic azole drug -8.7 kcal/mol). The investigated ligands, Lupeol, Nyctanthic acid, Beta-amyrin, and Apigenin, interacted more significantly with fungal drug targets through hydrogen bonds and hydrophobic interactions. The structural assessment of the 5FSA-ligand complexes showed stability with root mean square deviation (RMSD) values between 0.2 and 0.4nm, also investigated through 500 ns molecular dynamics simulations, which considered different geometric properties and computed the binding free energy. We also observed significant ligand-receptor interactions and high drug-likeness properties for the observed molecules using the pkCSM absorption, distribution, metabolism, and excretion (ADMET) method.

This study suggested the screened phytochemicals of this plant, namely Lupeol, Nyctanthic acid, Beta-amyrin, and Apigenin, or their combination, could inhibit fungal pathogens and could be beneficial to control the fungal-mediated food spoilage and aspergillosis in both plants and animals. Nevertheless, more *in vitro* and *in vivo* research is required to validate these findings.

1. Introduction

Over recent decades, many pathogenic fungi, including species of *Aspergillus*, *Cryptococcus*, and *Candida*, have been reported to develop resistance mechanisms such as target site mutations, biofilm formation, and efflux pump overexpression, that significantly reported to significantly reduce the efficacy of currently used antifungal drugs. The consequence is a growing number of cases where infections become hard to treat, resulting in increased morbidity, mortality, and expensive healthcare. Alarmingly, some resistant strains are now considered multidrug-resistant, further complicating treatment options and emphasizing the urgent need for novel anti-fungal agents. The antifungal potentialities of phytometabolites have been primarily rooted in a specific class of molecules such as flavonoids, phenolics, alkaloids, terpenoids, and saponins. These compounds act through various mechanisms, including disrupting fungal cell membranes (allicin from garlic, eugenol from clove, which has also been reported to inhibit adenosine triphosphatase (ATPase) enzyme activity, while increased permeability has been explored with thymol, from thyme, and interfering with the synthesis of vital cell components like ergosterol.

However, resveratrol has been reported to inhibit fungal enzymes linked to the synthesis of the cell wall and disrupts membrane integrity to facilitate cell lysis. The previously reported inhibitory activities of phytochemicals against *Candida* and *Aspergillus spp.* stated that plant-based molecules could be comparable to, or even surpass, conventional synthetic antifungals in terms of antifungal spectrum and potency. Moreover, plant-derived antifungal agents have been incorporated into topical formulations, including ointments or creams, coatings, and as a natural preservative for many food items to stop fungal growth and deterioration, indicating their versatile application spectrum rooted in their chemical properties rather than traditional or general therapeutic contexts

Thus, plants are a promising reservoir of bioactive metabolites with significant antifungal potentialities, often reported to show multi-target mechanisms that can reduce resistance development. *Nyctanthes arbor-tristis* (*N. arbor-tristis*), a traditional medicinal plant rich in flavonoids, alkaloids, and phenolic compounds, has garnered attention due to its reported pharmacological properties, including antifungal activities in preliminary studies.

*Corresponding author:

E-mail address: m.quazi@qu.edu.sa (QMS Jamal)

Received: 23 October, 2025 Accepted: 04 January, 2026 Epub Ahead of Print: 04 April, 2026 Published: 16 April, 2026

DOI: 10.25259/JKSUS_1667_2025

N. arbor-tristis, belonging to the family *Oleaceae*, is a small, ornamental tree native to Southeast Asia and India. It is also known as parijat, harsingar, and night jasmine. It is well known for its fragrant white blooms that open only at night. The plant has been used for centuries in traditional Indian medicinal products due to its many health benefits. This plant has several health benefits, including its anti-inflammatory properties, which help patients cope with pain and inflammation. Due to their antipyretic properties, the plant contains compounds that can reduce fever. The plant's components include antioxidants, which can protect the body from damage caused by free radicals (Arendrup et al., 2014; Sana et al., 2024). The plant contains compounds with astringent properties that may help to tighten skin and reduce inflammation. Chemicals in the plant can break up mucus and ease coughing.

Additionally, laxative components of the plant have been reported, which may help relieve constipation due to their laxative properties. The plant has components that resemble sedatives and can help people relax mentally and physically. The night jasmine has also been reported to have antifungal properties against a variety of fungi, including *Malassezia furfur*, *Aspergillus niger*, and *Aspergillus flavus*. Some of the plant's compounds can damage fungi's cell walls, which will eventually cause the fungi to die. A few studies on the antimicrobial qualities of *N. arbor-tristis* have been carried out, including an evaluation of the plant's antifungal activity against *Aspergillus flavus* and *Aspergillus niger*. Previous studies have demonstrated that the ethanolic extract of *N. arbor-tristis* leaves effectively suppressed *Aspergillus flavus* and *Aspergillus niger*. According to reports, this extract can prevent up to 60% of the growth of tested fungi. (Das and Bhatnagar 2022, Gahtori et al., 2023). Studies on the anti-*Malassezia* properties of *Nyctanthes arbor-tristis* and their use in treating infections (Mishra et al., 2016). The Asia Pacific region now has 83% of its population resistant to azole antibiotics, and the emergence of resistant fungal strains poses a severe threat to crop protection, human health, and food spoilage. A methanolic extract from *N. arbor-tristis* flowers was previously shown to be effective against *Malassezia furfur*, a fungus that causes dandruff. The extract reduced this fungal's growth potential by up to 80%. *N. arbor-tristis* possesses antifungal qualities that can combat both *Candida albicans* (*C. albicans*) and *Aspergillus niger* (*A. niger*). Methanolic extract from the leaves of *N. arbor-tristis* is an effective way to combat *Candida albicans*, a fungus associated with yeast infections. The extract reduced the growth rate of this fungus by up to 70%.

Additionally, it has proven effective in inhibiting *A. niger* growth, halting its growth by up to 50%. The plant is thought to possess antifungal qualities due to compounds such as calceolarioside A, esitosterol, and quercetin. *In vitro*, these compounds have significant antifungal activity. The antifungal qualities of *N. arbor-tristis* have drawn more interest lately. Numerous studies have demonstrated the antifungal activity of extracts from the plant's leaves, flowers, and bark against *Aspergillus flavus*, *A. niger*, and *Malassezia furfur* (Sharma et al., 2023).

Nonetheless, these studies' findings suggest that plants are a potential natural remedy for fungal infections. It's critical to remember that *N. arbor-tristis* is a medicinal product and should only be used by qualified medical professionals. (Kumari and Charya 2016, Sharma et al., 2023).

Lupeol, a pentacyclic triterpenoid, beta amyryl, and Nyctanthic acid are commonly found in various medicinal plants, including *N. arbor-tristis*. These phytochemicals garnered attention for their potent pharmacological properties, including antibacterial and antifungal, which are primarily attributed to their ability to interact with the fungal cell membrane.

An important development in medicinal chemical research is the integration of computational techniques, molecular docking, dynamics, and simulation into the search for new bioactive compounds, including antifungal agents from natural resources. Traditionally, exploring natural chemicals for antifungal efficacy is laborious and resource-intensive due to their complexity. The use of cheminformatics technologies has accelerated the discovery process through virtual screening, predictive modelling, and data analysis of extensive collections of natural compounds, aiding in the identification of lead candidates and the understanding of their structure-activity relationships. Molecular docking, dynamics, and simulations have been reported to provide

comprehensive insights into how screened phytochemicals interact with fungal targets, including their binding potential and mechanisms of interaction. Compounds such as berberine, curcumin, and eugenol have been reported to show computationally predicted antifungal activity against many pathogenic fungi. Combining these approaches has allowed for a more efficient and targeted exploration of natural chemical diversity, which is especially important given the rise of drug resistance and the limited availability of new therapies. This integrated approach enhances the discovery of novel antifungal agents from natural resources and offers a promising pathway toward innovative, sustainable treatments and improved global health.

This study analyzed the interaction of *N. arbor-tristis*'s chemicals using cheminformatics tools with the used drug targets for fungi, pathogenic yeast *C. albicans* (PDB:5FSA) (Hargrove et al., 2017), *A. fumigatus* protein farnesyltransferase (PDB: 4LNG) (Mabanglo et al., 2014), the crystal structure of lanosterol 14-alpha demethylase (PDB:5EQB) (Monk et al., 2014), and the fungal chitinase from *A. fumigatus* (PDB:2XUC) (Rush et al., 2010) were used. The plant contains various compounds with potential medical uses, such as anti-inflammatory, anti-arthritis, and anti-cancer agents (Bhadra, 2020). Nevertheless, more research needs to be conducted on the chemical makeup of antifungal agents and their interactions. Prior extensive computational analysis demonstrated that arbortristiside E and beta-sitosterol, natural constituents of this plant, exhibited substantial binding affinity towards cyclooxygenase-1 (COX-1), cyclooxygenase-2 (COX-2), phosphodiesterase-4 (PDE4), phosphodiesterase-7 (PDE7), interleukin-17A (IL-17A), interleukin-17D (IL-17D), tumor necrosis factor-alpha (TNF- α), interleukin-1 beta (IL-1 β), prostaglandin E2, and prostaglandin F synthase (Ahmad et al., 2023).

To demonstrate the protection against fungal strains, this study aimed to investigate the most essential interacting antifungal molecules that could target the sterol 14-alpha demethylase, an important enzyme required for life-supporting processes in fungal strains. This study used molecular docking to investigate the antifungal interactions between the target protein of fungal strains linked to fungal growth and natural compounds from *N. arbor-tristis*. The results of this study could be hypothesized that compounds like lupeol and Nyctanthic acid from this plant could be used as antifungals to manage food, agriculture, and health-associated fungal problems.

2. Materials and Methods

2.1 Natural compounds preparation

Simplified molecular input line entry system (SMILES) is one of the features of 2-dimensional (2D) structures. The structural files for the most critical natural compounds of *N. arbor-tristis* were obtained from the PubChem database (Kim et al., 2016), and the file for Drug posaconazole (DB01263) was obtained from the DrugBank database (Wishart et al., 2008). 2D structures of selected compounds were generated from the SMI2Depict online tool (<https://cdb.ics.uci.edu/cgi-bin/SMI2DepictWeb.py>) (Chen et al., 2007) (Supplementary material S1). It utilized the Novoprolab server to get SMILES IDs and transform them into 3D format for docking and simulation needs from Protein Databank (PDB) format (Burley et al., 2022). The discovery studio visualizer also processed the generated ligand files to minimize energy. To treat macromolecular systems as, the Chemistry at Harvard macromolecular mechanics 27 (CHARMm27) forcefield was used to carry out an energy minimization process that indicates the functional empirical energy (Brooks et al., 1983; Bjelkmar et al., 2010).

2.2 Target receptor preparation

The crystal structure of sterol 14-alpha demethylase (cytochrome P450 enzyme (CYP51)), which is shown in combination with the antifungal medication posaconazole from the pathogenic yeast *C. albicans* (PDB:5FSA) (Hargrove et al., 2017), *A. fumigatus* protein farnesyltransferase (PDB: 4LNG) (Mabanglo et al., 2014), the crystal structure of lanosterol 14-alpha demethylase (PDB:5EQB) (Monk et al., 2014), and the structure of fungal chitinase from *A. fumigatus* (PDB:2XUC) (Rush et al., 2010) were curated and downloaded from

the PDB database. We have eliminated the water molecules and hetero atom (HETATM) from the published structures and applied the CHARMM27 force field for energy minimization to prepare the downloaded 3D crystal structure for docking studies. The amino acid residues in the active site of selected receptors that interact with the HETATM present in the native PDB structures were discovered during the investigation and visualized in the Discovery Studio Visualizer 2021 version 21.1.0.20298 (Biovia 2021). The active-site amino acid residues' coordinates were extracted from the native structure, and then docking studies were conducted using these residues in the binding pocket. All receptor biomolecules were rendered in 3D using Discovery Studio Visualizer 2021 version 21.1.0.20298 (Biovia 2021).

2.3 Molecular docking studies

The binding affinities between natural compounds and the selected antifungal targets were estimated using AutoDock 4.2, an MGL tool (Morris et al., 2009). For interaction studies, the Lamarckian genetic algorithm (L.G.A.) was employed (Morris et al., 1998). Using molecular docking techniques, the optimal conformation of receptors with drug compound complexes was examined after calculating binding energy (G) with the following formula.

$$\Delta G_{\text{binding}} = \Delta G_{\text{gauss}} + \Delta G_{\text{repulsion}} + \Delta G_{\text{hbond}} + \Delta G_{\text{hydrophobic}} + \Delta G_{\text{tors}}$$

In this instance, the dispersion of two Gaussian functions has an attractive term of ΔG_{gauss} . Repulsion: if the distance is less than a certain threshold, the square of the distance ramp function for ΔG_{hbond} : also applied to interactions between metal ions $\Delta G_{\text{hydrophobic}}$: ramp characteristic, ΔG_{tors} : represents the number of bonds that can be rotated (Morris et al., 2008, Morris et al., 2009).

Also, Ligand efficacy (LE) was calculated by the formula;

$$LE = \Delta G_{\text{binding}} / \text{No of Heavy atoms}$$

Furthermore, the water molecules extracted from the chosen 3D native structures were given hydrogen atoms, gasteiger charge, Kollman united charges, and solvation parameters before docking. The X, Y, and Z axes of a grid point's grid box values were set to 60x60x60°. The grid's point spacing was initially set to 0.375. The flexible docking analysis between compounds and protein molecules was carried out using the L.G.A. The L.G.A. parameters set by default were 0.8 and 0.2, respectively. These included the 150 population size (ga_pop_size), the 2500000 energy evaluations (ga_num_generation), the 27000 mutation rate, the 0.02-crossover rate, and the step size. Ten runs were used to select the L.G.A. Analysis was done on the receptor-ligand complex conformations. Discovery studio visualizer was used to render 3D and 2D conformations of ligand and receptor complexes.

2.4 Drug-likeness and absorption, distribution, metabolism, and excretion (ADMET)

Using the Swiss ADME online tool (<http://www.swissadme.com>), the Swiss Institute of Bioinformatics (S.I.B.), Lausanne, Switzerland, provided computational predictions of the ADME, drug-likeness, and pharmacokinetics properties of a subset of natural compounds (Daina et al., 2017). Additionally, using the web server for pharmacokinetics of small molecules server (pkCSM) (Pires et al., 2015). SwissADME drug-likeness criteria were based on Lipinski's Rule of Five: molecular weight ≤ 500 Da, $\text{LogP} \leq 5$, hydrogen bond donors ≤ 5 , and hydrogen bond acceptors ≤ 10 . Additional filters like Ghose, Veber, Egan, and Muegge were also considered (e.g., rotatable bonds ≤ 10 , total polar surface area (TPSA) $\leq 140 \text{ \AA}^2$). Compounds violating more than one rule were regarded as less drug-like. For pkCSM ADMET predictions, the cut-offs included intestinal absorption $\geq 30\%$, Caco-2 permeability $\text{logPapp} > 0.9$, blood-brain barrier permeability $\text{logBB} > 0.1$, and toxicity flags such as non-mutagenic in Ames mutagenicity (AMES) test and absence of hepatotoxicity.

2.5 Molecular dynamics simulation (MDS)

The docking results for the lupeol, nycanthic acid, beta-Amyrin, and control drug (DB01263)-receptor complexes needed further MDS evaluation. As a result, simulations for these complexes were set up in the MDS environment to run for 100 nanoseconds (ns). In addition, we simulated the protease in water for a comparison of the results using the 2018 version of the Groningen machine for chemical simulations (GROMACS) tool developed in 2005 by the Netherlands' Groningen University (Van Der Spoel et al., 2005).

The pdb2gmx module was used to create the required PDB:5FSA topology file, after which the CHARMM27 all-atom force fields were selected. CHARMM27 remains widely used and supported in many simulation packages, offering a good balance of accuracy and computational efficiency for our study (Bjellmar et al., 2010). In the next step, topology files for the ligands lupeol, nycanthic acid, beta-Amyrin, and control medication DB01263 were created using the SwissParam server (Zoete et al., 2011). A unit cell triclinic box filled with water was made for the solvation step. Energy was decreased after Na^+ and Cl^- ions were added to the system to stabilize it. Once the system (selected complexes) had reached equilibrium, two-step ensembles, N.V.T. (constant number of particles, pressure, and temperature) and N.P.T. (constant number of particles, pressure, and temperature), were used. Through rigorous simulation, both ensembles control the temperature and pressure coupling, leading to consistency and stabilization of the system (Gupta et al., 2020). The gmx rms package was utilized to analyze complex trajectory files. It computes the root mean square deviation (RMSD) [gmx rms] (Kufareva and Abagyan 2012), the root mean square fluctuation (RMSF) [gmx rmsf], the radius of gyration (Rg) [Gmx gyrate] [(Kuzmanic and Zagrovic 2010), and the gmx hbnum for hydrogen-bond formation rates calculation during the interaction. 2D plots were created with the Xmgrace software version 5.1.19 (Turner 2005). Furthermore, the Molecular mechanics-poisson-Boltzmann surface area (MM-PBSA) method (Kollman et al., 2000) Based free energy calculations were executed after utilizing molecular mechanics poisson-boltzmann surface area (MMPBSA).py Python script developed by Miller et al., 2012 (Miller et al., 2012). The free energy calculation is finally run by the gmx_MMPBSA program (Valdés-Tresanco et al., 2021). It accommodates various solvation models, binding energy decomposition, and entropy corrections, while maintaining computational efficiency. gmx_MMPBSA facilitates GPU acceleration, hence considerably enhancing the speed of calculations for extensive systems. These features render it highly appropriate for our investigation and facilitate precise, efficient outcomes.

The scoring function formula used by the gmx_MMPBSA method is based on the principle of MMPBSA. The binding free energy (G_{bind}) is calculated as follows:

$$\Delta G_{\text{bind}} = G_{\text{complex}} - (G_{\text{receptor}} + G_{\text{ligand}})$$

where each G (free energy) term is composed of molecular mechanics and solvation energy contributions:

$$G = E_{\text{MM}} + G_{\text{solvation}} - TS$$

Here:

- E_{MM} : Molecular mechanics energy (bonded + electrostatic + van der Waals terms)
- $G_{\text{solvation}}$: Solvation free energy (polar and nonpolar contributions; polar calculated via PB or GB, nonpolar typically via SASA)
- TS : Entropy term (often omitted for relative binding calculations)

The expanded formula for binding free energy without entropy is:

$$\begin{aligned} \Delta G_{\text{bind}} &= \Delta E_{\text{MM}} + \Delta G_{\text{solvation}} \\ \Delta E_{\text{MM}} &= \Delta E_{\text{internal}} + \Delta E_{\text{electrostatic}} + \Delta E_{\text{vdW}} \\ \Delta G_{\text{solvation}} &= \Delta G_{\text{polar}} + \Delta G_{\text{nonpolar}} \end{aligned}$$

So, the full formula is:

$$\Delta G_{bind} = \left[\Delta E_{internal} + \Delta E_{electrostatic} + \Delta E_{vdW} \right] + \left[\Delta G_{polar} + \Delta G_{nonpolar} \right]$$

These molecular mechanics energies combined with solvation were calculated by SASA models and Poisson-Boltzmann from GROMACS MD trajectories.

Principal component analysis (PCA) was carried out by Gromacs command *gmx trjconv*, *gmx covar*, and *gmx ana eig*, and free energy landscape (FEL) analysis was also carried out. FEL 3D plots were created by a Python script *freeEnergyLandscape.py* developed by Leon (Sulfriery 2024).

3. Results and Discussion

Traditional antifungal strategies have long served as the cornerstone of managing fungal infections, with agents such as azoles, polyenes, and echinocandins being commonly employed clinically with some limitations, including toxicity, a narrow spectrum of activity, and less effectiveness against certain resistant strains. Polyenes such as amphotericin B are potent antifungals but cause severe nephrotoxicity, infusion-related adverse reactions, drug-drug interactions, and poor penetration, limiting their prolonged use.

Over recent decades, many pathogenic fungi, including species of *Aspergillus*, *Cryptococcus*, and *Candida*, have developed resistance mechanisms such as target site mutations, biofilm formation, and efflux pump overexpression that have been reported to significantly reduce the efficacy of currently used antifungal drugs. The consequence is a growing number of cases where infections become hard to treat, resulting in increased morbidity, mortality, and expensive healthcare. Alarmingly, some resistant strains are now considered multidrug-resistant, further complicating treatment options and emphasizing the urgent need for novel anti-fungal agents. Natural products have historically been a rich source of antimicrobials, including antifungal agents, and offer diverse biological activities and chemical structures that synthetic drugs may lack. Plants are a promising reservoir of bioactive metabolites with significant antifungal potentialities, often reported to show multi-target mechanisms that can reduce resistance development. *N. arbor-tristis*, a traditional medicinal plant rich in flavonoids, alkaloids, and phenolic compounds, has garnered attention due to its reported pharmacological properties in preliminary studies. The cheminformatics-based results of this study were observed to be significant.

The top three compounds were selected for additional research after we sifted and shortened the harsingar natural compounds based on our determined binding affinity as compared to the control drug binding affinity (Supplementary material S2). Also, Ligand efficacy (LE) was calculated, and all ligands showed efficacy ranging from -0.14 to -0.42 kcal/mol/atom (Supplementary material S3). Also, the 2D and 3D visualization patterns depicted in Figs. 1(a-t) between PDB:5FSA, 4LNG, 5EQB, and 2XUC, as well as selected natural compounds, including control drug DB01263.

In the crystal structure of sterol 14-alpha demethylase (CYP51) from the pathogenic yeast *Candida albicans* (5FSA), the binding affinity, hydrogen bonds, length of hydrogen bonds, and amino acid residues involved in van der Waals and other interactions of four different ligands are displayed in Table 1 and Figs. 1(a-t). Removing the amino acid group 14alphamethyl from lanosterol is a crucial step in the biosynthesis of ergosterol, which is necessary for the membranes of fungal cells. This process is catalyzed by the CYP51. CYP51 is also primarily targeted by clinical antifungals like azoles, which bind to heme iron in the active site to inhibit its activity.

The selected natural compound, lupeol, a triterpene compound present in different plants, has the highest binding affinity (-11.5 kcal/mol). Nyctanthic acid, a naturally occurring product from *Nyctanthes arbor-tristis*, comes in second place with -10.3 kcal/mol. The lowest binding affinity is -8.7 kcal/mol for DB01263, a synthetic azole drug, while another triterpene compound, beta-amyrin, has a binding affinity of -9.8 kcal/mol. According to these findings, beta amyrin and DB01263 are less effective CYP51 inhibitors than lupeol and nyctanthic acid (Table 1).

Figs. 1(g and h) demonstrated how two hydrogen bonds with LYS143 and HIS468, which have respective lengths of 2.70749 and 3.08699, form nyctanthic acid in CYP51-activated sites. Compared to nyctanthic acid and DB01263, lupeol and beta-amyrin have more amino acid residues involved in van der Waals interactions. Still, they do not form hydrogen bonds or interact with CYP51 (Figs. 1a-f). Three hydrogen bonds have been included in DB01263 by TYR505, SER507, and MET508, consisting of 2.70749, 3.08699, or 3.09413. Furthermore, DB01263 forms a pi-sulfur interaction with MET508 and a pi-pi stacked interaction with TYR118 (Figs. 1g and h). The effect of this interaction could be felt in DB01263's CYP51 specificity and selectivity. These interactions may improve the ligand-protein complex's hydrophobicity and stability, as depicted in Fig. 1. Beta-amyrin was observed to interact more strongly with binding affinity -9.0 Kcal/mol than the studied control drugs (-8.5 Kcal/mol). The interaction was mediated through the involvement of one Hydrogen bond: UNK1:H63 and B: ASP430:OD1, and through Van der Waals interaction of amino acid residues: LEU147, TRP153, TRP157, TRP371, ASP430, TYR432, and TYR436. Lupeol-5eqb complex was stabilized with significant binding energy(-10 Kcal/mol), which Van der Waals interactions of amino acid LEU147, TRP153, TRP157, TRP371, ASP430, TYR432, and TYR436 could facilitate. The Binding affinity of -8.4 kcal/mol was observed with the Apigenin-2xuc complex. Hydrogen bonds facilitated the complex: Forms hydrogen bonds between A: ASN62:HD21 and UNK1:O20. Van der Waals interaction amino acid residues: ASN76, GLN37, TYR125, PHE60, GLY123, ASP172, TYR232, and ASN233.

In the center is a ball stick pattern that displays all compounds. The interacting amino acid residues were shown as a pink stick pattern in 3D visualization and a sphere colored according to their interaction in 2D visualization. Remainders forming hydrogen bonds are displayed in dark green, while residues involved in the Van der Waals interaction are shown in light green. Also, light and dark pink hues indicated Pi-Pi stacking and Pi-Pi/Pi-alkyl interacting residues—a purple sphere displaying the remnants of the Pi-sigma bond. Various colored dotted lines illustrate the bond types that arise during compound interaction. An overview of the positions of ligands within CYP51's active site and how they interact with heme groups and amino acid residues can be seen in 3D images. The two-dimensional representations display the schematic diagrams of the ligands and their interactions with CYP51. Various interactions, including hydrogen bonds, van der Waals contacts, pi-alkyl, pi-sigma, and pi-pi stacking interactions, are indicated by different colors and symbols. 2D representations help compare the similarities and differences between ligands and visualize binding modes.

The figure shows that the triterpene compound lupeol originated from various plants, has a complex structure, and binds to almost all CYP51's active sites. PHE233, HIS468, TYR132, LEU139, LEU300, ILE304, GLY303, PHE126, THR122, GLY307, and PHE233 are among the amino acid residues with which it forms multiple van der Waals contacts. Additionally, it interacts pi-alkyl with TYR118, MET508, ILE131, LEU121, PHE228, TYR118, LYS143, and ILE471 (Figs. 1a and b). Smaller and more flexible than lupeol, nyctanthic acid is a compound in *Nyctanthes arbor-tristis*. It interacted twice with LYS143 and HIS468 in CYP51's active region. Through van der Waals forces, it is also connected to GLY303, GLY308, GLY307, PHE126, PHE228, LEU139, ARG469, CYS470, and TYR132. It interacts through alkyl/pi-alkyl interactions with LEU376, LEU121, ILE304, and ILE471. It also forms a pi-sigma interaction with TYR118 (Figs. 1c and d).

Although the structures of lupeol and beta-amyrin, another triterpene compound, are similar, some differences exist in the conformation and orientation of the rings. It forms van der Waals contacts with GLY472, GLY308, GLY307, PHE126, THR122, GLY303, and ILE131. It forms a pi-sigma interaction with TYR118. It forms alkyl/pi-alkyl interaction with ILE304, ILE471, CGS470, TYR132, LEU376, PHE228, and LEU121 (Figs. 1e and f). DB01263, a synthetic azole medication, is significantly smaller and has a simpler structure than the other three ligands. It forms three hydrogen bonds with TYR505, SER507, and MET508 in the CYP51 active site. Together with GLY308, GLY307, LYS143, LEU139, GLY472, LEU204, PHE475, ILE471, ALA146, THR122, PHE228, PRO230, LEU87, SER378, PHE233, LEU121, and ILE379, it also creates van der Waals contacts. It forms a pi-sulfur interaction with MET508

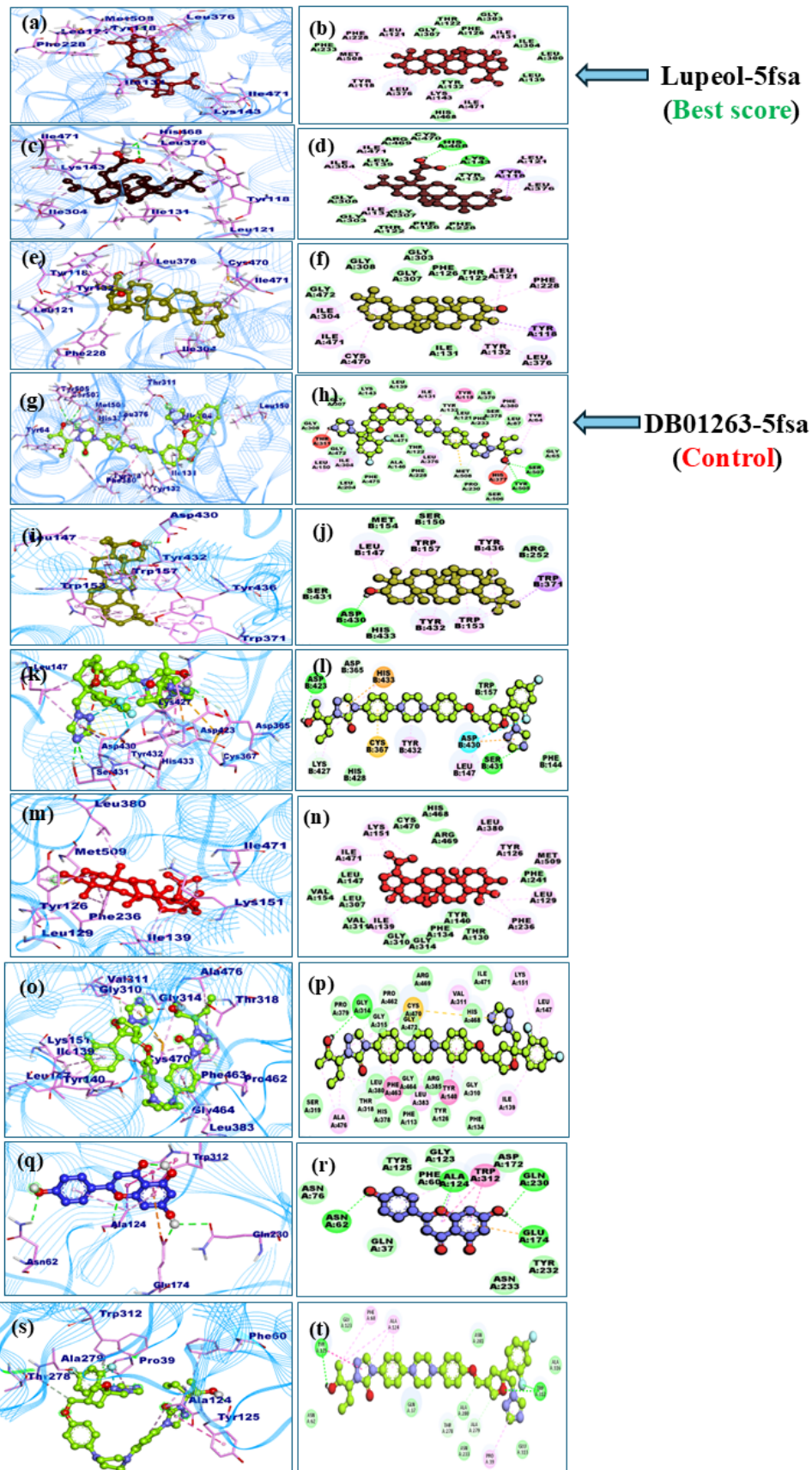


Fig. 1. Representation of 3D and 2D conformation of complexes (a-b) Lupeol-5fsa, (c-d) Nyctanthic acid-5fsa, (e-f) Beta-amyrin-5fsa, (g-h) DB01263-5fsa, (i-j) Beta-amyrin-4lng, (k-l) DB01263-4lng, (m-n) Lupeol-5eqb, (o-p) DB01263-5eqb, (q-r) Apigenin-2xuc, and (s-t) DB01263-2xuc. In the 3D visualization, all receptor molecules are represented by a blue-wired ribbon pattern with interacting ligands Lupeol (red), Nyctanthic acid (maroon), Beta-amyrin (olive), and control drug DB01263 (green). In 2D figures, interacting amino acid residues are colored by their bonding type: hydrogen bonds (green), Van der Waals (light green), Alkyl/Pi-alkyl (light pink), Pi-Pi T-shaped (dark pink), Pi-sigma (purple), Pi-sulfur (yellow), Halogen-fluorine (sky), Pi-anion/cation (orange), and unfavorable donor-donor (red).

Table 1.

The molecular docking data were obtained during the interaction between PDB:5FSA,4LNG,5EQB, and 2XUC and selected natural compounds, including the control drug DB01263.

Complex	Binding affinity (Kcal/mol)	Hydrogen bonds	Length of hydrogen bonds	Amino acid residues involved in the Van der Waals interaction	Amino acid residues involved in other interactions
Lupeol-5fsa	-11.5	Na	NA	PHE233,HIS468, TYR132,LEU139, LEU300,ILE304, GLY303,PHE126, THR122,GLY307, PHE233	Pi-Alkyl=ILE131, LEU121,PHE228, MET508, TYR118, LEU376,LYS143, ILE471
Nyctanthic acid-5fsa	-10.3	A:LYS143:HZ1 - A:UNK1:O14	2.94646	GLY303,GLY308, GLY307,PHE126, PHE228,LEU139, ARG469,CYS470, TYR132	Pi-Sigma=TYR118, ALKYL/PI-ALKYL=LEU376, LEU121,ILE304, ILE471,ILE131
		A:UNK1:H51 - A:HIS468:O	2.24182		
Beta-amyrin-5fsa	-9.8	NA	NA	GLY472,GLY308, GLY307,PHE126, THR122,GLY303, ILE131	Pi-Sigma=TYR118 Alkyl/Pi-Alkyl= ILE304,ILE471, CYS470, TYR132, LEU376,PHE228, LEU121
DB01263-5fsa control	-8.7	:UNK0:H24 - A:TYR505:O	2.70749	GLY308,GLY307, LYS143,LEU139, GLY472,LEU204, PHE475,ILE471, ALA146,THR122, PHE228,PRO230, LEU87,SER378, PHE233,LEU121, ILE379,	Pi-Sulfur=MET508 Pi-Pi Stacked= TYR118 Alkyl/Pi-Alkyl= LEU376,ILE304, LEU150,ILE131, PHE380, TYR64
		:UNK0:H24 - A:SER507:O	3.08699		
		:UNK0:C25 - A:MET508:O	3.09413		
		A:TYR132:HH - :UNK0	3.15579		
Beta-amyrin-4lng	-9.0	:UNK1:H63 - B:ASP430:OD1	1.70074	LEU147, TRP153, TRP157, TRP371, ASP430, TYR432, TYR436	Pi-Sigma=TRP271 Alkyl/Pi-Alkyl=LEU147, TRP157, TYR436, TRP153, TYR432
DB01263-4lng control	-8.5	B:SER431:HN - :UNL1:N7	2.45189	LEU147, ASP365, CYS367, ASP423, LYS427, ASP430, SER431, TYR432, HIS433	Pi-Sigma=ASP430 Halogen= ASP430 Pi-Anion= ASP430 Pi-Cation=HIS433 Pi-Pi T shaped=HIS433 Pi-Sulfur=CYS367 Alkyl/Pi-Alkyl=TYR432
		B:SER431:HG - :UNL1:N7	2.11493		
		:UNL1:H11 - B:ASP423:OD2	2.0774		
		B:LYS427:CE - :UNL1:O1	3.45509		
		:UNL1:C7 - B:ASP365:OD2	3.3862		
Lupeol-5eqb	-10.3	NA	NA	VAL154,LEU307, LEU147, VAL311, GLY310, GLY314, PHE134, TYR140, THR130, PHE241, ARG469, HIS468, CYS470	Pi-Alkyl= TYR126, LEU129, ILE139, LYS151, PHE236, LEU380, ILE471, MET509
DB01263-5eqb control	-11.8	:UNL1:H11 - A:GLY314:O	2.0999	SER319, PRO379, LEU380, HIS378, PHE113, GLY464, ARG385, TYR126, ARG385, PHE134, GLY315, ARG469, HIS468, ILE471	Pi-Pi T-shaped=TYR140 Amide-Pi Stacked=PHE463 Pi-Alkyl=ALA476, LEU383, ILE139, LEU147, LYS151, VAL311, Pi-Sulfur=470
		:UNL1:C7 - A:PRO462:O	3.32838		
		:UNL1:C3 - A:THR318:OG1	2.84777		
		:UNL1:C28 - A:GLY310:O	2.48001		
Apigenin-2xuc	-8.4	A:ASN62:HD21 - :UNK1:O20	2.71395	ASN76, GLN37, TYR125, PHE60, GLY123, ASP172, TYR232, ASN233	Pi-Sigma=ALA124, Pi-Pi Stacked=TRP312 Pi-Alkyl=Ala124 Pi-Anion=GLU174
		A:ALA124:HN - :UNK1:O17	2.09936		
		:UNK1:H28 - A:GLU174:OE2	1.90438		
		:UNK1:H28 - A:GLN230:OE1	2.79708		
DB01263-2xuc	-7.2	A:TRP312:HE1 - :UNL1:O4	2.22946	ASN62, GLN37, GLY123, ALA280, ASN281, GLU313, ALA316	Alkyl/Pi-Alkyl=PRO39, PHE60, ALA124, Pi-Pi Stacked=TYR125
		A:TRP312:HE1 - :UNL1:F1	2.30862		
		:UNL1:H11 - A:TYR125:O	1.97243		
		:UNL1:C24 - A:THR278:O	3.64401		
		:UNL1:C28 - A:ALA279:O	2.89213		

and a pi-pi stacked interaction with TYR118. Moreover, TYR64, LEU376, ILE304, LEU150, ILE131, PHE380, and ILE131 interact alkyl/pi-alkyl with (Figs. 1g and h). The synthetic azole drug DB01263, compared to the other three ligands, is significantly smaller and has a simpler structure. Three hydrogen bonds are formed by it with TYR505, SER507, and MET508 in the CYP51 active site. Together with GLY308,

GLY307, LYS143, LEU139, GLY472, LEU204, PHE475, ILE471, ALA146, THR122, PHE228, PRO230, LEU87, SER378, PHE233, LEU121, and ILE379, it also creates van der Waals contacts. When combined with MET508, it forms a pi-sulfur interaction; when combined with TYR118, it forms a pi-inverted pi interaction. Furthermore, it has alkyl/pi-

alkyl interactions with TYR64, ILE304, LEU150, ILE131, PHE380, and ILE131.

It has been noted that the four compounds beta-amyryn, DB01263 (control), lupeol, and nyctanthic acid interact within the same 5FSA active site. The same binding pocket that interacted with the control DB01263 under study also contained the interacting amino acids, such as Tyr118, Phe380, Leu87, and others. Van der Waals, hydrophobic, or hydrogen bonding interactions helped to promote the binding. It has been observed that nyctanthic acid, beta-amyryn, and lupeol bind at the same interaction region as the control drug (DB01263). Therefore, these compounds may have comparable therapeutic potential by modulating the activity of 5FSA ([Supplementary material S4](#)).

4. ADMET

The prediction for ADME is shown in ([Supplementary material S5](#)). SwissADME is an online resource that provides an extensive library of predictive models for various physicochemical, pharmacokinetic, and drug-likeness properties of small molecules. The ([Supplementary material S5](#)) compares the ADME characteristics of four different ligands that bind to the crystal structure of sterol 14-alpha demethylase (CYP51) from the pathogenic yeast *Candida albicans* (PDB:5FSA). The cytochrome P450 enzyme CYP51 catalyzes the removal of the 14-alpha-methyl group from lanosterol, a critical step in synthesizing ergosterol, an essential component of the fungal cell membrane. This protein is also the target of most clinical antifungal drugs, such as azoles, which bind to the heme iron in the active site of CYP51 to prevent it from functioning.

As shown in ([Supplementary material S5](#)), the synthetic azole drug DB01263 has a high gastrointestinal (G.I.) absorption rate, meaning that the intestinal mucosa can easily absorb and permit it to enter the bloodstream. However, DB01263 cannot penetrate the central nervous system and cross the blood-brain barrier (B.B.B.). DB01263 is a substrate of P-glycoprotein (Pgp), an efflux pump that facilitates the removal of medications from cells and tissues. This suggests that Pgp-mediated efflux could lead to DB01263, which has reduced bioavailability and drug resistance. Moreover, DB01263 inhibits several cytochrome P450 (CYP) enzymes, such as CYP1A2, CYP2C19, CYP2C9, CYP2D6, and CYP3A4. These enzymes are responsible for the breakdown of drugs and other xenobiotics in the liver and other tissues. This suggests that DB01263 may have adverse effects and drug-drug interactions by inhibiting the metabolism of other medications or endogenous substances. Finally, because of its low log Kp value (-7.32 cm/s), which denotes poor skin penetration, DB01263 cannot be applied topically. ([Supplementary material S5](#)) shows that natural products with similar structures and ADME properties include lupeol, nyctanthic acid, and beta-amyryn. Because of their low G.I. absorption, they are all poorly absorbed by the intestinal mucosa and have low oral bioavailability.

Moreover, they cannot enter the central nervous system because they are not B.B.B. permeant. Since they are neither C.Y.P. nor Pgp enzyme substrates nor inhibitors, they are less likely to be affected by efflux or metabolism because of their low log Kp values (-1.9 cm/s for lupeol, -2.45 cm/s for nyctanthic acid, and -2.41 cm/s for beta-amyryn) and poor skin penetration.

([Supplementary material S5](#)) shows that beta-amyryn, nyctanthic acid, and lupeol have low skin penetration, B.B.B. permeation, and G.I. absorption. ([Supplementary material S5](#)) shows that the synthetic azole drug DB01263, in contrast to the other three ligands, has poor drug-likeness properties. According to Lipinski's rule of five, the high molecular weight (M.W.) of DB01263 is 700.78 g/mol, which is greater than the range of most medications (between 150 and 500 g/mol).

Furthermore, DB01263 has twelve rotatable bonds, exceeding Veber's rule, which states that most drugs have nine or fewer rotatable bonds. DB01263 has a low bioavailability score of 0.17, less than the reasonable oral bioavailability threshold of 0.25. DB01263 has a moderate synthetic accessibility score of 6.02, meaning it is not easy to synthesize.

([Supplementary material S6](#)) shows that natural products with properties resembling those of pharmaceuticals include beta-amyryn, nyctanthic acid, and lupeol. With a moderate molecular weight (M.W.) of 400–500 g/mol, each of them defies Lipinski's rule, though this does

not necessarily mean that they cannot be drugs. They all comply with Veber's rule and have low rotatable bonds (0 to 4), indicating good oral bioavailability. They all have low numbers of donors and acceptors of hydrogen bonds (1 to 2), which means good membrane permeability according to Lipinski's rule. All drugs have a common TPSA between 20 and 40 Å², which violates Egan's rule, which states that most drugs have a TPSA between 20 and 130 Å². Low TPSA, however, can also be a sign of low solubility and good membrane permeability. They all have moderate to high bioavailability scores, ranging from 0.55 to 0.85, which indicates good oral bioavailability. None are straightforward to synthesize, with scores for average synthetic accessibility ranging from 5.49 to 6.04.

([Supplementary material S7](#)) predicts several toxicity endpoints, including AMES mutagenicity, maximum tolerated dose (M.T.D.) in humans, human ether-a-go-go related gene (hERG) inhibition, oral rat acute and chronic toxicity, hepatotoxicity, skin sensitization, *Tetrahymena pyriformis* toxicity, and minnow toxicity. The ([Supplementary material S7](#)) also shows the standard cut-off values for each endpoint that indicate a high risk of toxicity. The data originated from the pkCSM server, a web-based platform providing a vast collection of prediction models for small molecules' physicochemical, pharmacokinetic, and toxicological characteristics.

([Supplementary material S7](#)) indicates that DB01263, a synthetic azole drug, has moderate to high toxicity when compared to the other three ligands. DB01263 is not an AMES mutagenic agent because it does not harm D.N.A. or result in mutations in bacteria. However, DB01263's high M.T.D. of 0.682 log(mg/kg/day) exceeds the cut-off value of 0.477 log(mg/kg/day), implying a small safety margin in humans. DB01263 is also categorized as an hERG II inhibitor because it inhibits the hERG potassium channel, which regulates the cardiac action potential and may cause cardiac arrhythmias or sudden death. The drug (DB01263) has a moderate oral rat acute toxicity threshold, meaning that after a single oral administration, 3.076 log(mg/kg) is the dose at which 50% of rats die. DB01263 has the lowest recorded adverse effect level after repeated oral administration for 28 days, with a low oral rat chronic toxicity (LOAEL) of 0.198 log(mg/kg/day).

Furthermore, DB01263 is hepatotoxic, meaning it causes harm to the liver or liver malfunction. DB01263 is not a skin sensitizer because it does not result in allergic contact dermatitis or skin inflammation—50% of *T. pyriformis* growth at a given concentration. The low *T. pyriformis* toxicity of DB01263 (0.285 log(ug/L)), a unicellular ciliated protozoan used as a model organism for environmental toxicity testing, is inhibited. With a 50% lethal concentration at -3.711 log(LC50) for minnows, a small freshwater fish used as a model organism for aquatic toxicity testing, DB01263 has a very low minnow toxicity.

([Supplementary material S7](#)) shows that beta-amyryn, nyctanthic acid, and lupeol are natural products with low to moderate toxicity and similar structures to DB01263. None induces hERG I inhibition, AMES mutagenesis, or skin sensitization. Their low M.T.D.s, ranging from -0.502 to -0.072 log(mg/kg/day), all indicate high human safety margins. They all have moderate oral rat acute toxicities, falling between 2.478 and 2.563 log(mg/kg), which means moderate doses kill 50% of rats after a single oral administration. They all have high oral rat chronic toxicities, ranging from 0.873 to 2.516 log(mg/kg/day), which indicate high doses that result in adverse effects after repeated oral administration for 28 days. Although lupeol and beta-amyryn are not hepatotoxic, nyctanthic acid is a Lopezine, and beta-amyryn is an hERG II inhibitor, but nyctanthic acid is not. Nyctanthic acid is a CYP2C9 inhibitor; lupeol and beta-amyryn are not. All of their low *T. pyriformis* toxicities fall between 0.292 and 0.383 log(ug/L), which indicates low concentrations that inhibit 50% of *T. pyriformis* growth. They all have moderate minnow toxicities, falling between -1.345 and -1.696 log(LC50), which indicates average concentrations that kill 50% of minnows. The ([Supplementary material S7](#)) provides valuable information about the toxicity properties of different CYP51 ligands, which can help evaluate their potential as antifungal drugs or lead compounds for drug discovery. The ([Supplementary material S7](#)) shows that DB01263 has moderate to high toxicity based on its high M.T.D., hERG II inhibition, hepatotoxicity, and low minnow toxicity. The table shows that acute and chronic oral rat toxicities, *T. pyriformis* toxicities, and low M.T.D.s of beta-amyryn, nyctanthic acid, and lupeol indicate

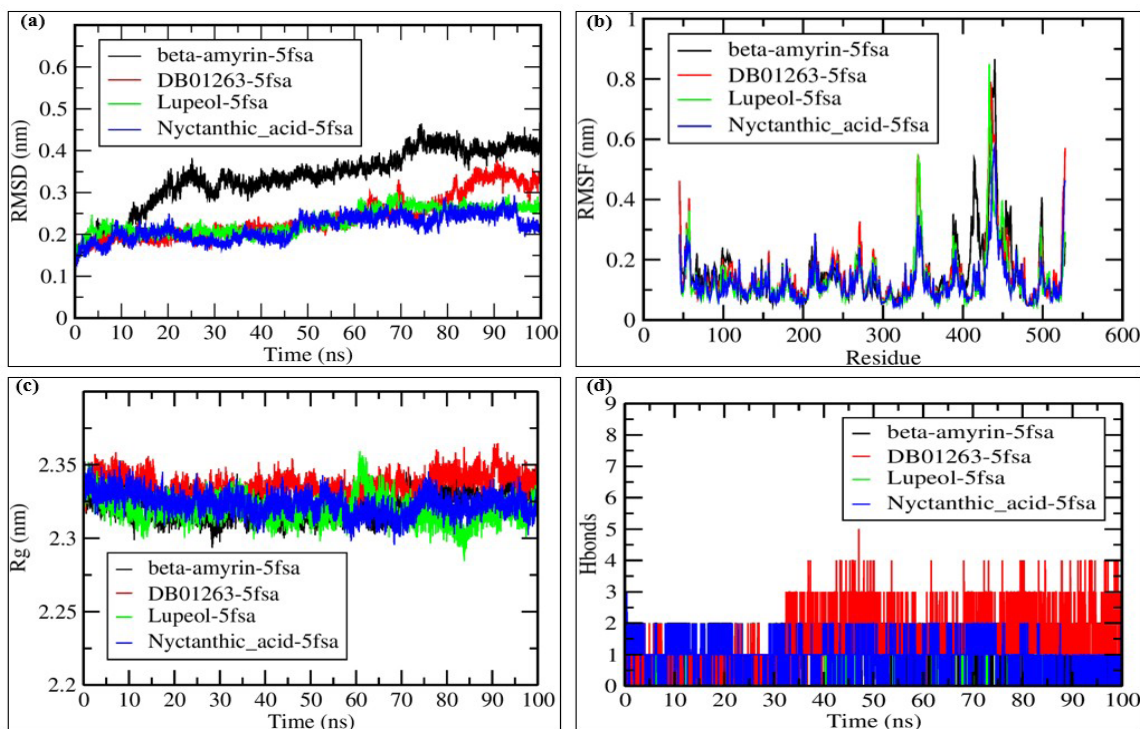


Fig. 2. 2D representation of 5FSA simulation data extracted from trajectory files (a) RMSD plot, (b) RMSF plot, (c) Radius of gyration plot, and (d) Hydrogen bonds plot formation of hbonds during 100ns simulation. Where ns = nanosecond. Different colors show natural compound patterns: Beta-amyrin (black), Lupeol (green), control drug DB01263 (red), and nyctanthic acid (blue).

low to moderate toxicity. However, they have some drawbacks, such as hepatotoxicity, CYP2C9 inhibition, mild minnow toxicities, and hERG II inhibition.

5. Molecular Dynamics and Simulation

We ran 100 ns simulations with a controlled drug and a 5fsa, 4lng, 5eqb, and 2xuc simulation for the best-chosen complexes. Also, we have

extended the 5FSA complex simulation to 500ns. All of the simulated complexes' RMSD values were found to vary between 0.2 and 0.4 nm (Fig. 2a). Except for a sudden increase fluctuating at a value of 0.3 nm that happened in the presence of the drug molecule after 80 ns of simulation, the 5fsa complexes with lupeol, the control drug DB01263, and nyctanthic acid exhibited similar values of less than 0.2 nm for the entire simulation period. According to the data, nyctanthic acid and lupeol are more stable than the control medication when interacting with 5fsa. The highest value was displayed by beta-amyrin-5fsa, which

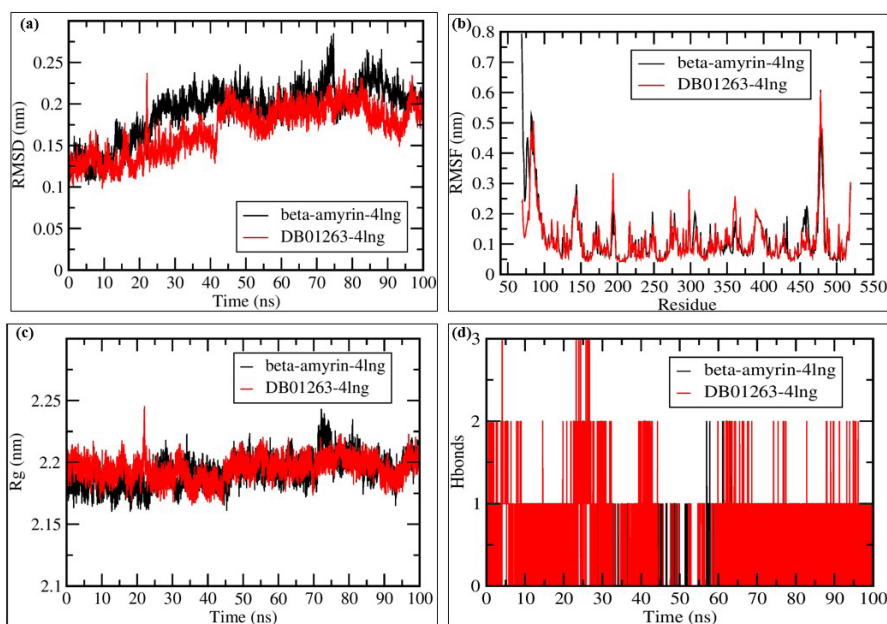


Fig. 3. 2D representation of 4LNG simulation fluctuation patterns (a) RMSD plot, (b) RMSF plot, (c) Radius of gyration plot, and (d) Hydrogen bonds plot formation of bonds during 100ns simulation. Where ns = nanosecond. Natural compounds Beta-amyrin (black) and control drug DB01263 (red).

began at 0.3 nm and ended the simulation at 0.4 nm. The values in the RMSF plot ranged from 0.1 to 0.8 nm. It was observed that all complexes nearly displayed a value of 0.1 nm, with amino acid regions 350–360 and 440–475 exhibiting the highest fluctuation (Fig. 2b).

The gyration plot's radius, ranging from 2.3 to 2.35 nm, displays a consistent pattern (Fig. 2c). The beta-amyrin, lupeol, and nyctanthic acid complexes all showed values close to 3.2 nm, substantially less than the 3.35 nm value of the control medication, DB01263. For every complex, the hydrogen bond plot (Fig. 2d) displays the formation of 1–5 hydrogen bonds. During the simulation, it was found that while nyctanthic acid formed two hydrogen bonds, the control drug, DB01263, formed five hydrogen bonds.

beta-amyrin-4lng and DB01263-4lng have shown fluctuations over time, with values ranging between approximately 0.15 and 0.25 nm (Fig. 3a). Both complex simulations showed similar patterns, with an average value of 0.15 after reaching the stable state after 40 ns, but the DB01263-4lng complex stayed below beta-amyrin-4lng. beta-amyrin-4lng and DB01263-4lng have shown RMSF values between 0.1 and 0.25nm during the complete simulation (Fig. 3b). Radius of gyration (Rg) calculation leads to assessing the compactness of receptor biomolecules. beta-amyrin-4lng followed the DB01263-4lng fluctuation pattern and showed values ranging between approximately 2.15 and 2.25 nm, while both molecules showed an average value of 2.2nm until the end of the simulation (Fig. 3c). The binding of receptors and ligands leads to the formation of hydrogen bonds. Also, the hydrogen bond plot shows the number of hydrogen bonds formed during the 100ns simulation. beta-amyrin-4lng complex formed 1-2 hydrogen bonds while DB01263-4lng formed 1-3 (Fig. 3d).

Lupeol-5eqb and DB01263-5eqb have shown fluctuations in RMSD over time in nanoseconds. The RMSD values for both complexes fluctuate between approximately 0.1 and 0.5 nm over the 100 ns period. Both complexes show similar patterns, but DB01263-5eqb generally stays below Lupeol-5eqb with 0.2nm, while Lupeol-5eqb shows an average value of 0.3nm (Fig. 4a). Apigenin-2xuc and DB01263-2xuc displayed RMSF for amino acid residues ranging between 0.2-0.4nm. Both datasets remain below 2 nm and very close to 0.1nm for the simulation, indicating relatively stable fluctuations (Fig. 4b). The radius of gyration (Rg) measures the compactness of a molecule. The overall values for Rg were between 2.5 and 2.75nm. Lupeol-5eqb and DB01263-5eqb complexes showed average fluctuation between 2.55 and 2.6 nm over a 100 ns simulation period (Fig. 4c). The hydrogen bond

plot represented the formation of hydrogen bonds during simulation. Lupeol-5eqb complex formed one hydrogen bond, while DB01263-5eqb formed 1-3 hydrogen bonds for the whole simulation period. The variation in hydrogen bond formation was observed at different time intervals (Fig. 4d). Apigenin-2xuc and DB01263-2xuc complexes RMSD plot showed an incremental pattern in the starting, but afterward stabilized at the end of the simulation Apigenin-2xuc showed an RMSD value near 0.15nm after reaching the stabilized state at 40ns simulation. DB01263-2xuc showed RMSD values near 0.1nm (Fig. 5a). RMSF analysis observed from the RMSF plot revealed that the overall value ranged from .05-0.45nm. Both complexes observed the highest peaks at amino acid regions 240-260. Both complexes showed similar average values of 0.05nm (Fig. 5b). Both compounds remained comparatively stable during an Rg value of 1.9nm throughout the observed period (Fig. 5c). DB01263-2xuc formed 1-3 hydrogen bonds, while Apigenin-2xuc formed 1-5 (Fig. 5d).

The obtained data of Poisson-Boltzmann complex energy and ligand-receptor energy components calculations were presented in [Supplementary materials S8 and S9](#):

The ΔG_{Total} value of -9309.00 (± 16.15) kcal/mol indicates intense binding energy for this complex. It would be interesting to compare it with other ligand-receptor interactions of the Lupeol-5fsa complex. Like Lupeol-5fsa, Nyctanthic acid-5fsa exhibits a substantial binding energy with a ΔG_{Total} of -9332.83 (± 17.54). The ΔG_{Total} value of -9388.77 (± 12.60) suggests a favorable interaction for Beta-amyrin-5fsa. The DB01263-5fsa control complex has a ΔG_{Total} of -9378.26 (± 23.37) ([Supplementary material S8](#)). It is a reference point for evaluating the other complexes [[Supplementary material S8](#)].

MMPBSA calculation of the whole complex of other receptors was also calculated. It was observed that Lupeol-5eqb showed ΔG_{Total} binding energy -10093.81 (± 9.67) kcal/mol. DB01263-5eqb control also showed the approximately very close ΔG_{Total} -10153.05 (± 9.33) kcal/mol, the lowest binding affinity. Nyctanthic acid-5fsa complex showed ΔG_{Total} -9332.83 (± 17.54), Beta-amyrin-5fsa showed ΔG_{Total} -9388.77 (± 12.60), and control complex DB01263-5fsa showed almost similar ΔG_{Total} -9378.26 (± 23.37) kcal/mol. Beta-amyrin-4lng and DB01263-4lng control complexes were shown very near ΔG_{Total} , i.e., -7214.29 (± 7.91) and -7125.83 (± 9.32) kcal/mol, respectively. Apigenin-2xuc showed a slightly higher ΔG_{Total} -3247.56 (± 13.93) than the DB01263-2xuc control complex -3192.70 (± 36.31). Overall,

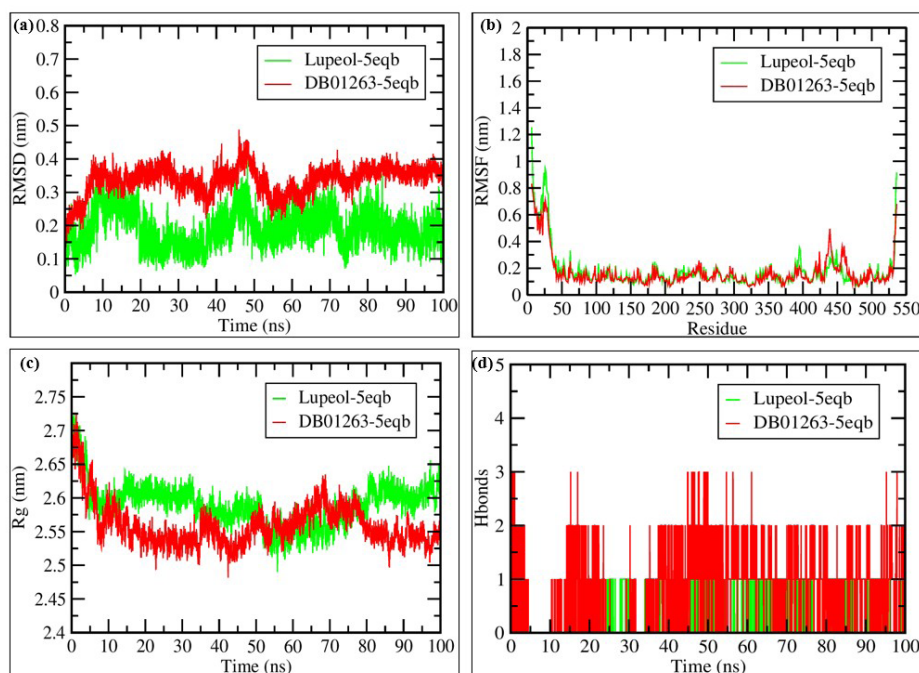


Fig. 4. 2D representation of 5EQB dynamics simulation data (a) RMSD plot, (b) RMSF plot, (c) radius of gyration plot, and (d) Hydrogen bonds plot formation of hbonds during 100ns simulation. Where ns = nanosecond. The natural compound is Lupeol (green), and the control drug is DB01263 (red).

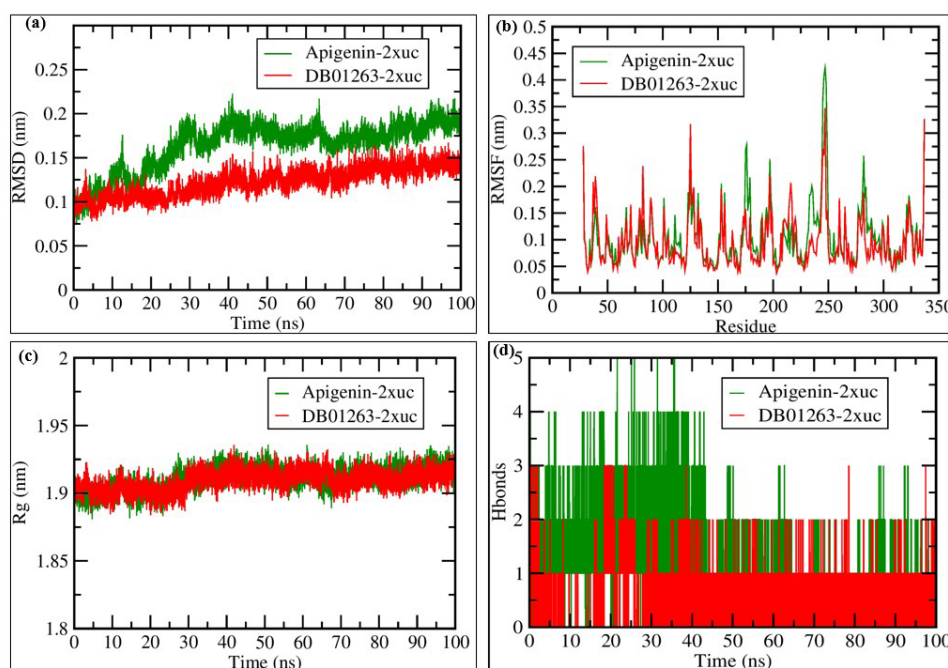


Fig. 5. 2D representation of 5XUC simulation patterns (a) RMSD plot, (b) RMSF plot, (c) Radius of gyration plot, and (d) Hydrogen bonds plot formation of hbonds during 100ns simulation. Where ns = nanosecond. Natural compound Apigenin (dark green), and control drug DB01263 (red).

the Lupeol-5eqb and DB01263-5eqb control complexes have shown significant binding energies, while Apigenin-2xuc and DB01263-2xuc have the least binding affinity.

Four complexes' total binding energy (ΔG_{Total}) indicates the binding is significant. However, the magnitude of the binding energy varies between the complexes. Lupeol-5fsa has the most favorable binding energy, followed by DB01263-5fsa-control, Beta-amyrin-5fsa, and Nyctanthic acid-5fsa. The Van der Waals energy (ΔV_{dw}) for all four complexes indicates attractive van der Waals interaction between the ligands and receptors. The electrostatic molecular energy (ΔE_{EL}) is negative for all four complexes, indicating attractive electrostatic interactions between the ligands and receptors. The solvation energy (ΔG_{Solv}) is positive for all four complexes, suggesting a penalty for transferring the ligands from the gas phase to the solvent. However, the solvation energy is less favorable for Lupeol-5fsa and DB01263-5fsa-control, which may contribute to their more favorable binding energies. The results obtained for the ligand-receptor complexes: Lupeol-5fsa, Nyctanthic acid-5fsa, Beta-amyrin-5fsa, and DB01263-5fsa-control. This value indicates a favorable binding energy of $-26.35 (\pm 0.74)$ for Lupeol-5fsa. It suggests strong interactions between the ligand and receptor. Like Lupeol-5fsa, Nyctanthic acid-5fsa exhibits a negative binding energy of $-31.69 (\pm 1.57)$ kcal/mol. The complex appears stable. Beta-amyrin-5fsa has shown comparable behavior. Its binding energy is also favorable, with the obtained value $-28.47 (\pm 0.58)$ kcal/mol. The control complex DB01263-5fsa has less negative binding energy $-12.45 (\pm 4.93)$ kcal/mol. It serves as a reference point.

Furthermore, we have also analyzed the ligand-receptor free energy calculation of other antifungal receptors' energetic components. Lupeol-5eqb complex $\Delta G_{\text{Total}} -28.70 (\pm 0.44)$ has shown a favorable binding affinity due to Van der Waals forces and reasonable solvation energy contribution. Nyctanthic acid-5fsa complex shown $\Delta G_{\text{Total}} -31.69 (\pm 1.57)$ kcal/mol, reflecting more stable interaction, like Lupeol-5eqb, but with slightly less negative values. The other complex, Beta-amyrin-5fsa and DB01263-5eqb control complexes show $\Delta G_{\text{Total}} -28.47 (\pm 0.58)$ and $-38.63 (\pm 0.71)$ kcal/mol, respectively, where the control complex has better interaction. Interestingly, Beta-amyrin-4lng showed $-29.81 (\pm 0.38)$ kcal/mol binding affinity, which is significantly higher than DB01263-4lng control binding energy, i.e., $-9.56 (\pm 0.50)$ kcal/mol. Apigenin-2xuc has shown $\Delta G_{\text{Total}} -9.48 (\pm 0.36)$ kcal/mol, which is a less favorable binding energy as compared to the control complex DB01263-2xuc shown $\Delta G_{\text{Total}} = -19.07 (\pm 0.43)$ kcal/mol. Overall,

the most substantial interaction is seen in the DB01263-5eqb control complex. This interaction has the highest overall binding energy ($\Delta G_{\text{Total}} = -38.63 \pm 0.71$). Three complexes interacted well as compared to DB01263 in terms of binding interactions, with higher ΔG_{Total} values, namely Lupeol-5eqb $\Delta G_{\text{Total}} -28.70 (\pm 0.44)$, Nyctanthic acid-5fsa $-31.69 (\pm 1.57)$, Beta-amyrin-5fsa $-28.47 (\pm 0.58)$. [Supplementary material S9]. These complexes have higher binding affinities, implying more persistent interactions with their target receptors. Also, β -Amyrin-4lng has better interactions than the DB01263-4lng control. β -Amyrin-5fsa has better interactions than the DB01263-5fsa control, which establishes β -Amyrin as a potential antifungal agent from studies of *Nyctanthes arbor-tristis* compounds.

5.1 5FSA 500ns extended MDS, PCA, and FEL

The RMSD plot was used to analyze the stability of the protein-ligand complexes. The beta-amyrin-5fsa (black) was observed to be the lowest deviation (~ 0.2 nm), and the complex conformational structure remains unchanged over time, supporting the system's more excellent structural stability and equilibrium state. However, Nyctanthic acid-5fsa (blue) was observed to have the highest fluctuations (~ 0.35 – 0.4 nm), indicating possible instability. The control (DB01263, red) and lupeol-5fsa (green) exhibited moderate stability, with RMSD values around 0.25 – 0.3 nm, which signifies the potentiality of the beta-amyrin (Fig. 6a).

The RMSF plot was used to show residue-wise flexibility. The plot shows that Peaks correspond to highly flexible loop regions, while stable areas have lower RMSF values. These regions could undergo significant fluctuations or conformational changes throughout the critical simulation. High RMSF observed values indicate that these loops are flexible and may have the flexibility to move more freely. This flexibility could be necessary for the protein's function and help these loops adopt variable conformations required for binding to ligands or other proteins. The beta-amyrin-5fsa (black) complex displayed minimal fluctuations, indicating strong binding stability. All ligand-bound systems followed a similar fluctuation pattern, with minor differences in loop regions (\sim residue 350–450) (Fig. 6b). The Rg plot quantifies the tightly packed nature of the protein structure. A lower Rg value suggests a more folded conformation and stability. Beta-amyrin-5fsa (black) was observed with the lowest Rg (~ 2.3 nm), signifying its compact structure. Nyctanthic acid-5fsa (blue) showed slightly higher

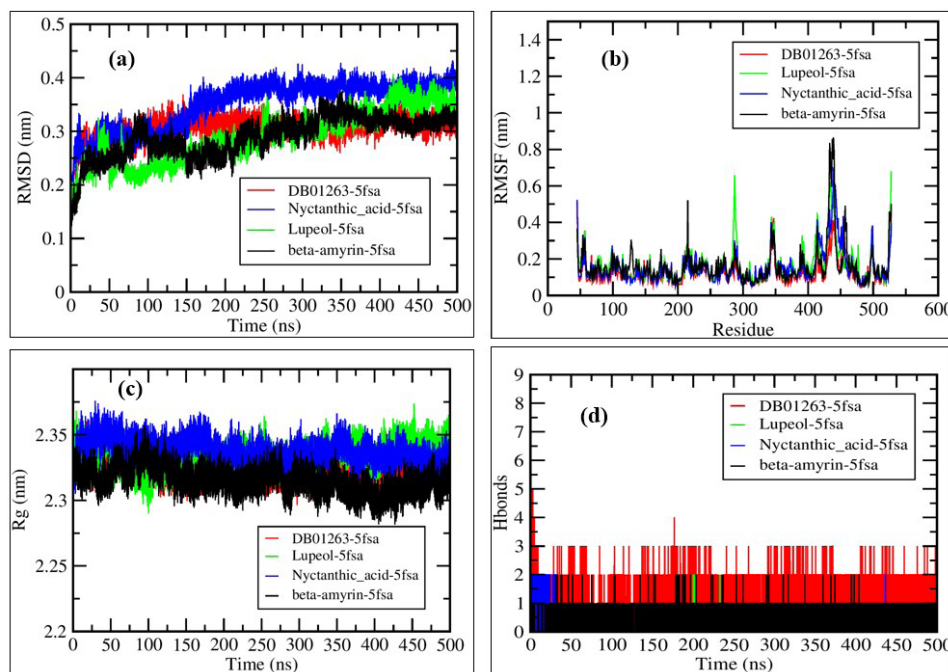


Fig. 6. Molecular dynamics (MD) simulation interactions analysis between selected ligand-protein complexes over 500 ns. (a) RMSD showing the structural stability of complexes. (b) RMSF explains the flexibility of each residue. (c) The radius of gyration (Rg) represents the compactness of the protein-ligand complexes. (d) Hydrogen bond analysis demonstrating the interaction stability between ligands and the target protein. Beta-amyrin-5fsa (black), control DB01263-5fsa (red), lupeol-5fsa (green), and nyctanthic acid-5fsa (blue) were compared.

Table 2.

Shows MMPBSA Calculations performed using 10,001 complex frames and Poisson-Boltzmann calculations performed using an internal PBSA solver in sander during a 500ns simulation.

Complex	Δ GGAS	Δ ASOL	Δ GTOTAL	SEM (Standard error mean)
Lupeol-5fsa	-48.85	16.12	-32.73	± 0.03
Nyctanthic acid-5fsa	-56.67	27.80	-28.80	± 0.04
beta-amyrin-5fsa	-57.42	24.17	-33.26	± 0.04
DB01263-5fsa control	-12.03	7.81	-12.03	± 0.11

Rg (~2.35 nm), implying a less compact system. The control and lupeol-5fsa followed similar trends (Fig. 6c). The number of hydrogen bonds determines ligand-protein interaction strength. The control (DB01263, red) formed the highest number of hydrogen bonds (~3–4 on average), suggesting strong interactions. Other ligands, including beta-amyrin-5fsa, formed fewer hydrogen bonds but remained stable over time (Fig. 6d).

Thus, Beta-amyrin has been found to exhibit the most stable and favorable binding energy, with fluctuations remaining within a lower range. Lupeol was also observed to be a relatively stable binding energy, though with slightly more fluctuations compared to beta-amyrin. Moreover, the complex exhibited the highest fluctuations and lowest favorable binding energy profile, suggesting weaker interactions. Among the studied data, the molecule beta-amyrin-5fsa demonstrated the highest stability, lowest fluctuations, compact structure, better efficacy, and less toxicity, making it proposing that it could be a strong candidate for further evaluation of its therapeutic potentialities. Also, MMPBSA analysis was conducted using the internal PBSA solver in sander at 10,001 most stable complex frames to determine the binding free energy of the used ligands to the receptor after extending the 500ns simulation. The binding free energy analysis revealed significant differences in ligand binding affinities. Among the tested ligands, beta-amyrin-5fsa exhibited the highest binding affinity with a Δ GTOTAL of -33.26 kcal/mol, followed closely by lupeol-5fsa (-32.73 kcal/mol) and nyctanthic acid-5fsa (-28.80 kcal/mol). The control ligand (DB01263-5fsa) showed a significantly weaker binding affinity (-12.03 kcal/mol), confirming the superior binding potential of the tested phytochemicals.

The gas-phase energy (Δ GGAS) for all test ligands was more than that of the control, indicating strong receptor-ligand interactions. However, the solvation energy (Δ GSOL) partially counteracted this effect, particularly in nyctanthic acid-5fsa, which showed the highest solvation energy penalty (27.80 kcal/mol). However, the ligand was observed to maintain a strong overall binding affinity (Table 2); (Supplementary material S10).

The low standard error values (ranging from 0.03 to 0.11) indicate the reliability of the binding free energy estimates. The results suggest that beta-amyrin-5fsa, lupeol-5fsa, and nyctanthic acid-5fsa could be potential lead compounds with enhanced receptor binding affinity compared to the control ligand (Table 2).

The PCA was conducted by using Gromacs trajectory files. PCA results indicated distinct clustering patterns for different ligand-bound systems, suggesting variations in conformational dynamics (Figs. 7a and b). DB01263-5fsa and Nyctanthic_acid-5fsa (blue) showed relatively compact distributions, while Beta-amyrin-5fsa (black) exhibited a more spread-out cluster, implying higher conformational flexibility (Fig. 7a). The eigenvalue spectrum in Fig. 7(b) shows that the first few eigenvectors contribute significantly to the overall motion, with a rapid decay in eigenvalues, indicating that most of the system's essential motions are captured by the first few principal components. This suggested that ligand binding affected the dominant motions of the system differently, influencing structural stability and flexibility.

Furthermore, the FEL analysis indicated significant variations in the conformational stability and flexibility of the ligand-bound complex. Beta-amyrin-5fsa and Lupeol-5fsa show multiple basins, explaining higher conformational variability and dynamic transitions between metastable states. The used control drug (DB01263-5fsa) showed a well-defined deep energy basin, supporting a stable binding conformation (Figs. 8a-c). Nyctanthic_acid-5fsa (indicated a different free energy minimum with a relatively broader basin, indicating moderate stability with some flexibility (Fig. 8d). FEL analysis revealed that ligand binding affected the free energy landscape, with DB01263-5fsa representing the most stable conformation, while other studied molecules permit greater conformational adaptability.

Additionally, the convergence analysis of RMSD, RMSF, Rg, and Energy based on the SAM analysis results confirmed the flexibility,

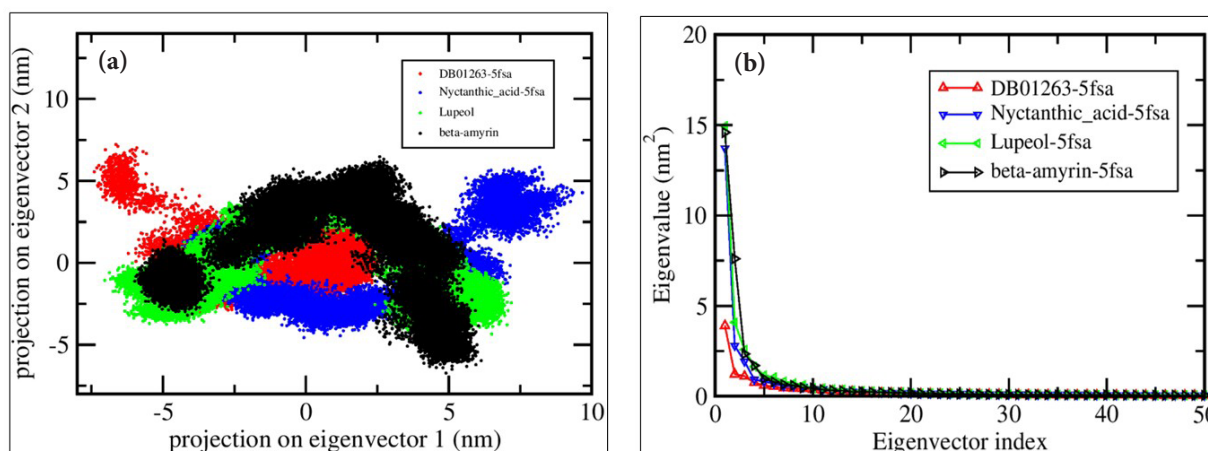


Fig. 7. PCA of MDS data from Ligand-5FSA systems. (a) Projection of molecular dynamics trajectories onto the first two principal components (eigenvectors) for four ligand-bound systems: DB01263-5fsa (red), Nyctanthic_acid-5fsa (blue), Lupeol-5fsa (green), and Beta-amyryn-5fsa (black). (b) Eigenvalue spectrum showing the contribution of each eigenvector to the overall system fluctuations.

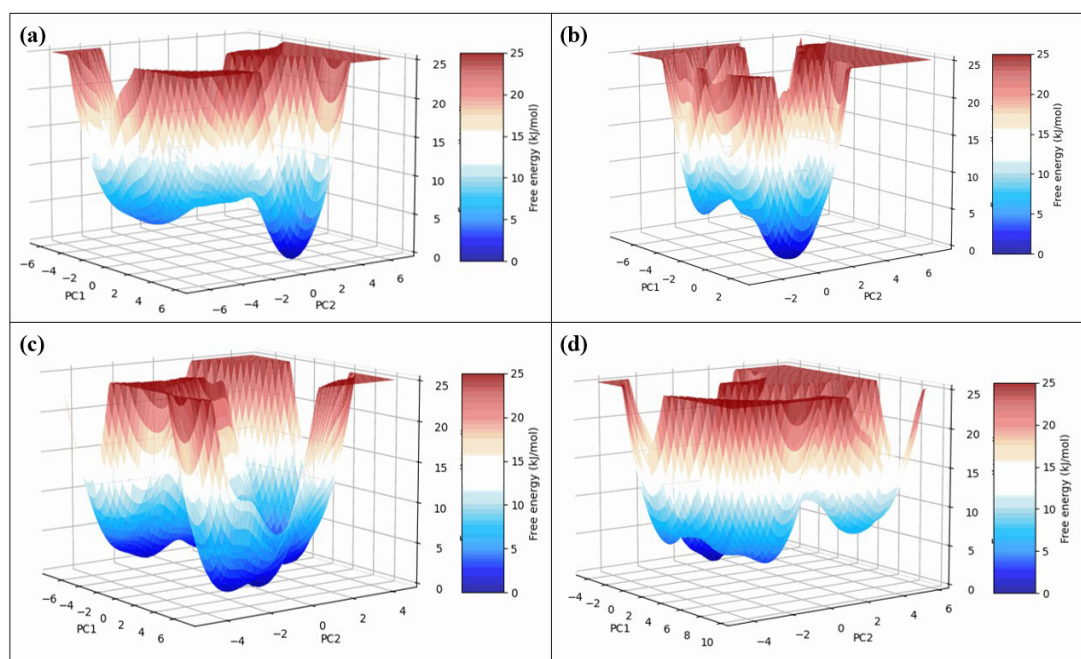


Fig. 8. 3D FEL Analysis of ligand-bound complex systems. The FEL maps show the conformational energy profile of ligand-bound systems along the first two principal components (PC1 and PC2). (a) Beta-amyryn-5fsa, (b) Control (DB01263)-5fsa, (c) Lupeol-5fsa, and (d) Nyctanthic acid-5fsa. The color gradient represents free energy (kJ/mol), where blue regions indicate energetically favorable (low free energy) conformational states and red regions represent high-energy states.

stability, and compactness of protein-ligand complexes during this analysis. The selected molecules confirm the binding stability, which is close to that of the positive control DB01263-5fsa, identified as the most stable complex. However, Nyctanthic acid-5fsa exhibited greater flexibility and a less compact structure ([Supplementary material S11](#)).

The CAM analysis accurately confirmed the complicated behaviors, which helped to improve the clarity of trend identification across different criteria. The pronounced stability and compactness of DB01263-5fsa and beta-amyryn-5fsa indicate beneficial and favorable interactions. The convergence of CAM-energy values across the complexes confirmed their equilibrium state and emphasized the predictability of the results we obtained ([Supplementary material S12](#)).

The prevalence of medication resistance, namely in the azole family of drugs used to treat fungal illnesses, is steadily increasing despite advancements in clinical understanding and treatment methods. This poses a significant threat to public health globally. Furthermore, miconazole, fluconazole, itraconazole, and ketoconazole have all been

associated with the development of acquired long QT syndrome [35] and cardiac arrhythmias, and the search for novel antifungal molecules is always desirable for the public health system. Chemicals and extracts from natural resources—plants, in particular—are required to treat fungal infections because they are the primary source of therapeutic molecules used in modern medicine. A common and ongoing threat to public health is fungal infections ([Kathiravan et al., 2012](#); [Ramirez et al., 2013](#)). Despite its well-established toxicities, the polyene antibiotic amphotericin B is often used to treat severe fungal infections ([Odds et al., 2003](#)). Due to prolonged exposure, drug interactions, and side effects like vision impairment, fluconazole is known to cause resistance to *Candida* species ([Canuto and Rodero 2002](#)) ([Chen and Sorrell 2007](#)). Resistance to commonly used antibiotics is increasing due to the increasing use of antifungal treatment, even in people who have never been exposed to the drug ([Arif et al., 2009](#); [Arendrup et al., 2014](#)). One of the most urgent problems facing therapeutics is the emergence of fungal strains resistant to antibiotics. Creating new antifungal

medications as soon as possible is crucial to address this issue (Johnson et al., 2007; Jianhua and Hai, 2009; Zorofchian Moghadamtousi et al., 2014). Creating novel active compounds and features depends heavily on utilizing natural resources. Natural substances as antifungal therapies provide excellent safety when employed with efficacy and precision in dosage, timing, and application method (Vengurlekar et al., 2012). Numerous bioactive secondary metabolites, such as tannins, saponins, alkaloids, terpenoids, flavonoids, and other compounds with antifungal properties, are found in plants (Arif et al., 2009). According to the study, the *N. arbor-tristis* plant has antifungal compounds, suggesting that the plant could develop into a novel antifungal medication that inhibits the enzyme responsible for synthesizing cell walls and could eventually replace the widely used antibiotics. Therefore, there is a need for new antifungal drugs with improved safety records, low side effects, lower costs, easier accessibility, and higher effectiveness against fungal infections. Encoded by a superfamily of genes, cytochromes, or P450 enzymes, are a class of heme-containing monooxygenases that are present in both prokaryotes and eukaryotes. These metabolizing enzymes aid the oxidation of pharmaceuticals, insecticides, and biosynthetic intermediates. They are also essential in activating a variety of carcinogens in eukaryotes. Most cytochromes P450 in mammals are found in the endoplasmic reticulum and are part of an intricate network that transports electrons. Cytochrome B6, Cytochrome B5, and Nicotinamide adenine dinucleotide phosphate (NADPH)-cytochrome P450 reductase are components of this system. Many distinct cytochrome P450 proteins are found in yeast and fungi, and the genes that produce these proteins have been found. Among them, *Saccharomyces cerevisiae's* lanosterol 14 α -demethylase (ERG1 1) has been investigated the most. This particular cytochrome P450 enzyme helps remove the methyl group from lanosterol at position C-32, an essential step in synthesizing ergosterol, a sterol present in yeast. The equivalent enzyme in mammals carries out the same reaction during cholesterol biosynthesis. Studies have supported this information (Aoyama et al., 1987, Yoshida 1988). Several antifungal medications, such as ketoconazole and itraconazole, specifically target lanosterol 14 α -demethylase (Vanden Bossche et al., 1986). Scientists exploited this property in their study to extract the *S. cerevisiae* ERG1 gene. To confer resistance to ketoconazole, they used a multicopy plasmid encoding lanosterol 14 α -demethylase (Kalb et al., 1986). Afterward, Kalb et al. presented a thorough sequence analysis of the gene and demonstrated its importance for aerobic growth (Kalb et al., 1987).

CYP51 inhibitors are highly beneficial antifungal medications, particularly effective against infectious fungi. Sterol 14- α -demethylase, often referred to as CYP51 or Lanosterol 14- α -demethylase, is an essential enzyme that plays a key role in the production of sterols, including cholesterol, in both prokaryotes and eukaryotes. (Singh et al., 2023) CYP51 has a crucial function in converting lanosterol to ergosterol, an essential element of fungal cell membranes. Its activity is a desirable target for antifungal drugs as it disrupts fungal membrane integrity, and didymellamides from plants have been described as CYP51 inhibitors. (Sama-ae et al., 2023), resulting in the death of the fungal cells. A variety of antifungal medicines generated from azoles function by selectively inhibiting CYP5112.

Farnesyltransferase is a catalytic protein that catalyzes the addition of a farnesyl group to the protein. Farnesyltransferase aids in protein prenylation in fungi, altering the location and function of proteins. (Kim et al., 2023). This enzyme could stop fungi from growing and sending signals. Researchers have studied farnesyltransferase inhibitors in the context of cancer, but are still considering their use against fungi. Chitinase is an enzyme that degrades chitin, a primary constituent of fungal cell walls. They break down chitin into smaller pieces through hydrolysis. Therefore, by explicitly targeting chitinases, the integrity of the fungal cell wall is disrupted. (Hu et al., 2023, Zhao et al., 2023), making the fungus susceptible to natural stress and immune system responses. Chitinase inhibitors have the potential to be created as antifungal pharmaceuticals. However, investigations into this field are still in progress. Many plant-derived phytochemicals have been

explored as potential antifungals. The phytochemicals of this plant have the potential to inhibit by targeting different cellular components of fungal cells. These enzymes have vital functions in producing necessary components inside fungal cells. Investigating plant-derived drugs that target these enzymes could offer valuable approaches to battling fungal infections. Additional research and medication development efforts are required to utilize their promise in clinical situations fully.

Complementary *in silico* docking analyses have further substantiated the results of this finding by revealing high binding affinities of lupeol to key fungal targets that could be involved in ergosterol biosynthesis, such as lanosterol 14 α -demethylase. These interactions suggest that lupeol may inhibit ergosterol synthesis, leading to impaired membrane formation and fungal cell death. Similarly, Nyctanthic acid, a phenolic compound derived from *Nyctanthes arbor-tristis*, has stated promising antifungal activity in recent studies. *In vitro* assays reported that that Nyctanthic acid effectively inhibited the growth of clinical isolates of *Candida* and *Cryptococcus* species. Molecular docking studies have provided insights into its mechanism, indicating strong binding affinity to fungal enzymes like chitin synthase and β -glucan synthase—key enzymes involved in the synthesis of cell wall components. By targeting these enzymes, Nyctanthic acid potentially hampers cell wall formation, rendering the fungi more susceptible to environmental stress and immune responses. Collectively, these recent *in silico* studies underscore the potential of lupeol and Nyctanthic acid as promising antifungal agents, acting through mechanisms that interfere with essential fungal biosynthetic pathways and structural integrity

6. Conclusions

Antifungal medications specifically target sterol 14- α demethylase, farnesyltransferase, lanosterol 14- α demethylase, and chitinase, critical proteins involved in the production of many cellular components of fungal cells, including ergosterol, a unique sterol that is exclusive to fungus, and chitinase Using investigated molecules Lupeol, Nyctanthic acid, Beta-amyrin, Apigenin, molecular docking, and dynamics simulation techniques were used to characterize the binding sites of target proteins. Our study's findings suggest that active compounds from this plant, like ketoconazole and itraconazole, have a strong affinity for a specific target interaction region. Intermolecular forces, such as hydrogen bonds, promote this binding and produce a significant binding energy to stabilize the protein-ligand complex. The studied compounds Lupeol, Nyctanthic acid, Beta-amyrin, and Apigenin have good drug-likeness attributes, as indicated by their low number of rotatable bonds, high bioavailability scores, and moderate molecular oral viability scores (MOVs). However, some of their shortcomings include their average synthetic accessibility ratings and poor TPSA. Moreover, despite cutting down on the cost of experimentation, computational studies need to be validated through *in vitro* and *in vivo* studies. Thus, the result of this study suggests that Lupeol, Nyctanthic acid, Beta-amyrin, and Apigenin could be significant anti-fungal agents that could be used to control many fungal-mediated food-crop spoilsages and animal diseases, including humans.

CRedit authorship contribution statement

Varish Ahmad: Conceptualization, data analysis, methodology, writing, review and editing; **Sohail Akhtar:** Conceptualization, data analysis, funding acquisition, writing, review and editing; **Qazi Mohammad Sajid Jamal:** Conceptualization, data analysis, funding acquisition, methodology; **Mohammad Aatif:** Writing, review and editing.

Declaration of competing interest

The authors declare that they have no known competing financial interests or personal relationships that could have appeared to influence the work reported in this paper.

Data availability

Data is contained within the article and the Supplementary material.

Declaration of generative AI and AI-assisted technologies in the writing process

The authors confirm that there was no use of artificial intelligence (AI)-assisted technology for assisting in the writing or editing of the manuscript, and no images were manipulated using AI.

Acknowledgment

This work was supported by the Deanship of Scientific Research, Vice Presidency for Graduate Studies and Scientific Research, King Faisal University, Saudi Arabia, Grant No: KFU254286.

Funding

This work was funded by the Deanship of Scientific Research, Vice Presidency for Graduate Studies and Scientific Research, King Faisal University, Saudi Arabia, [Grant No: KFU254286].

Supplementary data

Supplementary material to this article can be found online at https://dx.doi.org/10.25259/JKSUS_1667_2025.

References

- Ahmad, V., Khan, M.I., Jamal, Q.M.S., Alzahrani, F.A., Albiheyri, R., 2023. Computational molecular docking and simulation-based assessment of anti-inflammatory properties of *Nyctanthes arbor-tristis* Linn phytochemicals. *Pharmaceuticals (Basel)* 17, 18. <https://doi.org/10.3390/ph17010018>
- Aoyama, Y., Yoshida, Y., Sonoda, Y., Sato, Y., 1987. Metabolism of 32-hydroxy-24,25-dihydrolanosterol by purified cytochrome p-45014DM from yeast: evidence for contribution of the cytochrome to whole process of lanosterol 14 alpha-demethylation. *J Biol Chem* 262, 1239-1243. <https://pubmed.ncbi.nlm.nih.gov/3543000/>
- Arendrup, M.C., Cuenca-Estrella, M., Lass-Flörl, C., Hope, W.W., 2014. EUCAST technical note on *Candida* and micafungin, anidulafungin and fluconazole. *Mycoses* 57, 377-379. <https://doi.org/10.1111/myc.12170>
- Arif, T., Bhosale, J.D., Kumar, N., Mandal, T.K., Bendre, R.S., Lavekar, G.S., Dabur, R., 2009. Natural products-antifungal agents derived from plants. *J Asian Nat Prod Res* 11, 621-638. <https://doi.org/10.1080/10286020902942350>
- Bhadra, P., 2020. Efficacy of some compounds isolated from *Nyctanthes arbor-tristis* Linn. on human and plant diseases as revealed from in silico analysis. *Indian Journal of Natural Sciences*, 10(60), pp.20833-20839.
- BIOVIA, Dassault Systèmes. Discovery Studio Visualizer, v21.1.0.20298. San Diego, CA, USA: Dassault Systèmes; 2021.
- Bjellkmar, P., Larsson, P., Cuendet, M.A., Hess, B., Lindahl, E., 2010. Implementation of the CHARMM force field in GROMACS: Analysis of protein stability effects from correction maps, virtual interaction sites, and water models. *J Chem Theory Comput* 6, 459-466. <https://doi.org/10.1021/ct900549r>
- Brooks, B.R., Brucoleri, R.E., Olafson, B.D., States, D.J., Swaminathan, S., Karplus, M., 1983. CHARMM: A program for macromolecular energy, minimization, and dynamics calculations. *J Comput Chem* 4, 187-217. <https://doi.org/10.1002/jcc.540040211>
- Burley, S.K., Bhikadiya, C., Bi, C., Bittrich, S., Chao, H., Chen, L., Craig, P.A., Crichlow, G.V., Dalenberg, K., Duarte, J.M., Dutta, S., Fayazi, M., Feng, Z., Flatt, J.W., Ganesan, S.J., Ghosh, S., Goodsell, D.S., Green, R.K., Gurunovic, V., Henry, J., Hudson, B.P., Khokhriakov, I., Lawson, C.L., Liang, Y., Lowe, R., Peisach, E., Persikova, I., Piehl, D.W., Rose, Y., Sali, A., Segura, J., Sekharan, M., Shao, C., Vallat, B., Voigt, M., Webb, B., Westbrook, J.D., Whetstone, S., Young, J.Y., Zalevsky, A., Zardecki, C., 2022. RCSB Protein Data bank: Tools for visualizing and understanding biological macromolecules in 3D. *Protein Sci* 31, e4482. <https://doi.org/10.1002/pro.4482>
- Canuto, M.M., F.G. Rodero, 2002. Antifungal drug resistance to azoles and polyenes. *The Lancet infectious diseases* 2, 550-563.
- Chen, J.H., Linstead, E., Swamidass, S.J., Wang, D., Baldi, P., 2007. ChemDB update--full-text search and virtual chemical space. *Bioinformatics* 23, 2348-2351. <https://doi.org/10.1093/bioinformatics/btm341>
- Chen, S.C., Sorrell, T.C., 2007. Antifungal agents. *Med J Aust* 187, 404-409. <https://doi.org/10.5694/j.1326-5377.2007.tb01313.x>
- Daina, A., Michielin, O., Zoete, V., 2017. SwissADME: A free web tool to evaluate pharmacokinetics, drug-likeness and medicinal chemistry friendliness of small molecules. *Sci. Rep.* 7, 42717. <https://doi.org/10.1038/srep42717>
- Das, R. and Bhatnagar, S., 2022. Evaluation of *Nyctanthes arbor-tristis* for anti-fungal activity using *Aspergillus flavus* and *Aspergillus niger* as target experimental model. *World J Pharm Life Sci*, 8(7), pp.127-131. <https://www.wjpls.org/download/article/80062022/1656933167.pdf>
- Gahtori, R., Tripathi, A.H., Chand, G., Pande, A., Joshi, P., Rai, R.C., Upadhyay, S.K., 2024. Phytochemical screening of *nyctanthes arbor-tristis* plant extracts and their antioxidant and antibacterial activity analysis. *Appl Biochem Biotechnol* 196, 436-456. <https://doi.org/10.1007/s12010-023-04552-4>
- Gupta, S., Tiwari, N., Verma, J., Waseem, M., Subbarao, N., Munde, M., 2020. Estimation of a stronger heparin binding locus in fibronectin domain III14 using thermodynamics and molecular dynamics. *RSC Adv* 10, 20288-20301. <https://doi.org/10.1039/d0ra01773f>
- Hargrove, T.Y., Friggeri, L., Wawrzak, Z., Qi, A., Hoekstra, W.J., Schotzinger, R.J., York, J.D., Guengerich, F.P., Lepesheva, G.I., 2017. Structural analyses of *Candida albicans* sterol 14 α -demethylase complexed with azole drugs address the molecular basis of azole-mediated inhibition of fungal sterol biosynthesis. *J Biol Chem* 292, 6728-6743. <https://doi.org/10.1074/jbc.M117.778308>
- Hu, K., Li, R., Mo, F., Ding, Y., Zhou, A., Guo, X., Li, R., Li, M., Ou, M., Li, M., 2023. Natural product osthole can significantly disrupt cell wall integrity and dynamic balance of *Fusarium oxysporum*. *Pestic Biochem Physiol* 196, 105623. <https://doi.org/10.1016/j.pestbp.2023.105623>
- Jianhua, W., Hai, W., 2009. Antifungal susceptibility analysis of berberine, baicalin, eugenol and curcumin on *Candida albicans*. *J Med Colleges PLA* 24, 142-147. [https://doi.org/10.1016/s1000-1948\(09\)60030-7](https://doi.org/10.1016/s1000-1948(09)60030-7)
- Johnson, J.R., Sannes, M.R., Croy, C., Johnston, B., Clabots, C., Kuskowski, M.A., Bender, J., Smith, K.E., Winokur, P.L., Belongia, E., 2007. Antimicrobial drug-resistant *Escherichia coli* from humans and poultry products, Minnesota and Wisconsin, 2002-2004. *Emerg Infect Dis* 13, 838. <https://doi.org/10.3201/eid1306.061576>
- Kalb, V.F., Loper, J.C., Dey, C.R., Woods, C.W., Sutter, T.R., 1986. Isolation of a cytochrome p-450 structural gene from *Saccharomyces cerevisiae*. *Gene* 45, 237-245. [https://doi.org/10.1016/0378-1119\(86\)90021-1](https://doi.org/10.1016/0378-1119(86)90021-1)
- Kalb, V.F., Woods, C.W., Turi, T.G., Dey, C.R., Sutter, T.R., Loper, J.C., 1987. Primary structure of the P450 lanosterol demethylase gene from *Saccharomyces cerevisiae*. *DNA* 6, 529-537. <https://doi.org/10.1089/dna.1987.6.529>
- Kathiravan, M.K., Salake, A.B., Chotho, A.S., Dudhe, P.B., Watode, R.P., Mukta, M.S., Gadhwane, S., 2012. The biology and chemistry of antifungal agents: A review. *Bioorg Med Chem* 20, 5678-5698. <https://doi.org/10.1016/j.bmc.2012.04.045>
- Kim, J.H., Hildebrandt, E.R., Sarkar, A., Yeung, W., Waldon, R.A., Kannan, N., Schmidt, W.K., 2023. A comprehensive *in vivo* screen of yeast farnesyltransferase activity reveals broad reactivity across a majority of CXXX sequences. *G3 (Bethesda)* 13, jkad094. <https://doi.org/10.1093/g3journal/jkad094>
- Kim, S., Thiessen, P.A., Bolton, E.E., Chen, J., Fu, G., Gindulyte, A., Han, L., He, J., He, S., Shoemaker, B.A., Wang, J., Yu, B., Zhang, J., Bryant, S.H., 2016. PubChem substance and compound databases. *Nucleic Acids Res* 44, D1202-D1213. <https://doi.org/10.1093/nar/gkv951>
- Kollman, P.A., Massova, I., Reyes, C., Kuhn, B., Huo, S., Chong, L., Lee, M., Lee, T., Duan, Y., Wang, W., Donini, O., Cieplak, P., Srinivasan, J., Case, D.A., Cheatham, T.E., 2000. Calculating structures and free energies of complex molecules: Combining molecular mechanics and continuum models. *Acc Chem Res* 33, 889-897. <https://doi.org/10.1021/ar000033j>
- Kufareva, I., Abagyan, R., 2012. Methods of protein structure comparison. *Methods Mol Biol* 857, 231-257. https://doi.org/10.1007/978-1-61779-588-6_10
- Kumari, T. D. Sandhya, and M. A Singara Charya. 2016. "DOCKING STUDIES ON BIOACTIVE COMPOUNDS OF NYCTANTHES ARBOR-TRISTIS". *International Journal of Pharmacy and Pharmaceutical Sciences* 8 (5):361-65. <https://journals.innovareacademics.in/index.php/ijpps/article/view/10962>
- Kuzmanic, A., Zagrovic, B., 2010. Determination of ensemble-average pairwise root mean-square deviation from experimental B-factors. *Biophys J* 98, 861-871. <https://doi.org/10.1016/j.bpj.2009.11.011>
- Mabanglo, M.F., Hast, M.A., Lubock, N.B., Hellinga, H.W., Beese, L.S., 2014. Crystal structures of the fungal pathogen *Aspergillus fumigatus* protein farnesyltransferase complexed with substrates and inhibitors reveal features for antifungal drug design. *Protein Sci* 23, 289-301. <https://doi.org/10.1002/pro.2411>
- Masiá Canuto, M., Gutiérrez Rodero, F., 2002. Antifungal drug resistance to azoles and polyenes. *Lancet Infect Dis* 2, 550-563. [https://doi.org/10.1016/s1473-3099\(02\)00371-7](https://doi.org/10.1016/s1473-3099(02)00371-7)
- Miller, B.R., McGee, T.D., Swails, J.M., Homeyer, N., Gohlke, H., Roitberg, A.E., 2012. MMPBSA.py: An efficient program for end-state free energy calculations. *J Chem Theory Comput* 8, 3314-3321. <https://doi.org/10.1021/ct300418h>
- Mishra, R.K., Mishra, V., Pandey, A., Tiwari, A.K., Pandey, H., Sharma, S., Pandey, A.C., Dikshit, A., 2016. Exploration of anti-Malassezia potential of *Nyctanthes arbor-tristis* l. and their application to combat the infection caused by Mala s1 a novel allergen. *BMC Complement Altern Med* 16, 114. <https://doi.org/10.1186/s12906-016-1092-2>
- Moghadamtousi, S.Z., Kadir, H.A., Hassandarvish, P., Tajik, H., Abubakar, S., Zandi, K., 2014. A review on antibacterial, antiviral, and antifungal activity of curcumin. *Biomed Res Int* 2014, 186864. <https://doi.org/10.1155/2014/186864>
- Monk, B.C., Tomasiak, T.M., Keniya, M.V., Huschmann, F.U., Tyndall, J.D., O'Connell, J.D., Cannon, R.D., McDonald, J.G., Rodriguez, A., Finer-Moore, J.S., Stroud, R.M., 2014. Architecture of a single membrane spanning cytochrome P450 suggests constraints that orient the catalytic domain relative to a bilayer. *Proc Natl Acad Sci U S A* 111, 3865-3870. <https://doi.org/10.1073/pnas.1324245111>
- Morris, G.M., Goodsell, D.S., Halliday, R.S., Huey, R., Hart, W.E., Belew, R.K., Olson, A.J., 1998. Automated docking using a Lamarckian genetic algorithm and an empirical binding free energy function. *J Comput Chem* 19, 1639-1662. [https://doi.org/10.1002/\(SICI\)1096-987X\(19981115\)19:14%3C1639::AID-JCC10%3E3.0.CO;2-B](https://doi.org/10.1002/(SICI)1096-987X(19981115)19:14%3C1639::AID-JCC10%3E3.0.CO;2-B)
- Morris, G.M., Huey, R., Lindstrom, W., Sanner, M.F., Belew, R.K., Goodsell, D.S., Olson, A.J., 2009. AutoDock4 and AutoDockTools4: Automated docking with selective

- receptor flexibility. *J Comput Chem* 30, 2785-2791. <https://doi.org/10.1002/jcc.21256>
- Morris, G.M., Huey, R., Olson, A.J., 2008. Using AutoDock for ligand-receptor docking. *CP in Bioinformatics* 24. <https://doi.org/10.1002/0471250953.bi0814s24>
- Odds, F.C., Brown, A.J., Gow, N.A., 2003. Antifungal agents: Mechanisms of action. *Trends Microbiol* 11, 272-279. [https://doi.org/10.1016/s0966-842x\(03\)00117-3](https://doi.org/10.1016/s0966-842x(03)00117-3)
- Pires, D.E., Blundell, T.L., Ascher, D.B., 2015. pkCSM: Predicting small-molecule pharmacokinetic and toxicity properties using graph-based signatures. *J Med Chem* 58, 4066-4072. <https://doi.org/10.1021/acs.jmedchem.5b00104>
- Ramirez, J., Cartuche, L., Morocho, V., Aguilar, S., Malagon, O., 2013. Antifungal activity of raw extract and flavanons isolated from Piper ecuadorensis from Ecuador. *Revista Brasileira de Farmacognosia* 23, 370-373. <https://doi.org/10.1590/s0102-695x2013005000012>
- Rush, C.L., Schüttelkopf, A.W., Hurtado-Guerrero, R., Blair, D.E., Ibrahim, A.F.M., Desvergnès, S., Eggleston, I.M., van Aalten, D.M.F., 2010. Natural product-guided discovery of a fungal chitinase inhibitor. *Chem & Biol* 17, 1275-1281. <https://doi.org/10.1016/j.chembiol.2010.07.018>
- Sama-Ae, I., Pattarangoon, N.C., Tedasen, A., 2023. In silico prediction of antifungal compounds from Natural sources towards Lanosterol 14-alpha demethylase (CYP51) using Molecular docking and Molecular dynamic simulation. *J. Mol. Graph. Model.* 121, 108435. <https://doi.org/10.1016/j.jmgm.2023.108435>
- Sana, T., Khan, M., Siddiqui, B.S., Baig, T.A., Jabeen, A., Begum, S., Hadda, T.B., Shah, L., 2024. Anti-inflammatory and urease inhibitory iridoid glycosides from Nyctanthes arbor-tristis Linn. *J Ethnopharmacol* 319, 117368. <https://doi.org/10.1016/j.jep.2023.117368>
- Sharma, L., Dhiman, M., Dadhich, A., Sharma, M.M., Kaushik, P., 2023. Biogenic AgNPs Synthesized using Nyctanthes arbor-tristis L. fruit for antimicrobial dye degradation efficiencies. *J Saud University-Science* 35, 102614. <https://doi.org/10.1016/j.jksus.2023.102614>
- Singh, A., Singh, K., Sharma, A., Kaur, K., Chadha, R., Bedi, P.M.S., 2023. Recent advances in antifungal drug development targeting lanosterol 14 α -demethylase (CYP51): A comprehensive review with structural and molecular insights. *Chem Biol Drug Des* 102, 606-639. <https://doi.org/10.1111/cbdd.14266>
- Sulfierry, L., 2024. sulfierry/free_energy_landscape: v1.0.3 (v1.0.3). Zenodo. <https://doi.org/https://doi.org/10.5281/zenodo.10850229>
- Turner, P., 2005. XMGRACE, Version 5.1. 19. Center for coastal and land-margin research, oregon graduate institute of science and technology, Beaverton, OR. 2
- Valdés-Tresanco, M.S., Valdés-Tresanco, M.E., Valiente, P.A., Moreno, E., 2021. gmx_MMPBSA: A new tool to perform end-state free energy calculations with GROMACS. *J Chem Theory Comput* 17, 6281-6291. <https://doi.org/10.1021/acs.jctc.1c00645>
- Van Der Spoel, D., Lindahl, E., Hess, B., Groenhof, G., Mark, A.E., Berendsen, H.J., 2005. GROMACS: Fast, flexible, and free. *J Comput Chem* 26, 1701-1718. <https://doi.org/10.1002/jcc.20291>
- Vanden Bossche, H., Bellens, D., Cools, W., Gorrens, J., Marichal, P., Verhoeven, H., Willemsens, G., De Coster, R., Beerens, D., Haelterman, C., Coene, M.-Claire, Lauwers, W., le Jeune, L., 1986. Cytochrome p-450: Target for itraconazole. *Drug Dev Res* 8, 287-298. <https://doi.org/10.1002/ddr.430080133>
- Vengurlekar, S., Sharma, R., Trivedi, P., 2012. Efficacy of some natural compounds as antifungal agents. *Pharmacogn Rev* 6, 91-99. <https://doi.org/10.4103/0973-7847.99942>
- Wishart, D.S., Knox, C., Guo, A.C., Cheng, D., Shrivastava, S., Tzur, D., Gautam, B., Hassanali, M., 2008. DrugBank: A knowledgebase for drugs, drug actions and drug targets. *Nucleic Acids Res* 36, D901-D906. <https://doi.org/10.1093/nar/gkm958>
- Yoshida, Y., 1988. Cytochrome P450 of fungi: Primary target for azole antifungal agents. *Curr Top Med Mycol* 2, 388-418. https://doi.org/10.1007/978-1-4612-3730-3_11
- Zhao, L., Wang, J., Zhang, H., Wang, P., Wang, C., Zhou, Y., Li, H., Yu, S., Wu, R., 2023. Inhibitory effect of carvacrol against Alternaria alternata causing goji fruit rot by disrupting the integrity and composition of cell wall. *Front Microbiol* 14, 1139749. <https://doi.org/10.3389/fmicb.2023.1139749>
- Zoete, V., Cuendet, M.A., Grosdidier, A., Michielin, O., 2011. SwissParam: A fast force field generation tool for small organic molecules. *J Comput Chem* 32, 2359-2368. <https://doi.org/10.1002/jcc.21816>
- Moghadamtousi, S.Z., Kadir, H.A., Hassandarvish, P., Tajik, H., Abubakar, S., Zandi, K., 2014. A review on antibacterial, antiviral, and antifungal activity of curcumin. *Biomed Res Int* 2014, 186864. <https://doi.org/10.1155/2014/186864>